Main Manuscript for

Transcranial direct current stimulation modulates primate brain dynamics across states of consciousness

Guylaine Hoffner[a,1,*], Pablo Castro[a,b,1], Lynn Uhrig[a,c], Camilo M. Signorelli[d,e,f], Morgan Dupont[a], Jordy Tasserie[g], Alain Destexhe[b], Rodrigo Cofre[b,h], Jacobo Sitt[i,2] and Bechir Jarraya[a,j,2,*].

[a]Cognitive Neuroimaging Unit, CEA, INSERM, Université Paris-Saclay, NeuroSpin Center, 91191 Gif-sur-Yvette, France
[b]Institute of Neuroscience (NeuroPSI), Paris-Saclay University, Centre National de la Recherche Scientifique (CNRS), 91191, Gif-sur-Yvette, France
[c]Department of Anesthesiology and Critical Care, Necker Hospital, AP-HP, Université de Paris Cité, 75015, Paris, France
[d]Department of Computer Science, University of Oxford, Oxford, 7 Parks Rd, Oxford OUX1 3QG
[e]Laboratory of Neurophysiology and Movement Biomechanics (LNMB), Université Libre de Bruxelles (ULB), Route de Lennik 808, CP 640, Building N, campus Erasme, 1070 Brussels
[f]Center for Philosophy of Arstificial Intelligence, University of Copenhagen, Karen Blixens Plads 8, Copenhagen 2300, Denmark.
[g]Center for Brain Circuit Therapeutics, Department of Neurology, Brigham & Women's Hospital, Harvard Medical School, Boston, MA 02115, USA
[h]Laboratoire de Physique de l'École Normale Supérieure, CNRS, PSL University, Sorbonne Université and Université Paris Cité, 75005 Paris, France
[i]Sorbonne Université, Institut du Cerveau - Paris Brain Institute - ICM, Inserm, CNRS, Paris 75013, France
[j]Department of Neurology, Hopital Foch, 92150, Suresnes, France

[1]Co-first authors
[2]Co-last authors

*To whom correspondence should be addressed. Emails: guylaine.hoffner@inserm.fr; bechir.jarraya@cea.fr.

Author Contributions: G.H., L.U., J.S., and B.J. designed research; G.H., L.U., M.D., J.T. and B.J. performed research; G.H., P.C., L.U., C.M.S., A.D., R.C., J.S., and B.J. analyzed data; B.J. secured funding; and G.H., P.C. and B.J. wrote the paper and all authors contributed to its editing.

Competing Interest Statement: The authors declare no competing interest.

Keywords: tDCS, fMRI, brain dynamics, consciousness, prefrontal cortex.

Abstract

The resting primate brain is traversed by spontaneous functional connectivity patterns that show striking differences between conscious and unconscious states. Transcranial direct current stimulation, a non-invasive neuromodulatory technique, can improve signs of consciousness in disorders of consciousness, but can it influence conscious and unconscious dynamic functional connectivity? We investigated the modulatory effect of prefrontal cortex (PFC) transcranial direct current stimulation (tDCS) on brain dynamics in awake and anesthetized non-human primates using functional MRI. In awake macaques receiving either anodal or cathodal high-density tDCS (HD-tDCS), we found that cathodal stimulation robustly disrupted the repertoire of functional connectivity patterns, increased structure-function correlation, decreased Shannon entropy, and favored transitions towards anatomically-based patterns. Under deep sedation, anodal HD-tDCS significantly altered brain pattern distribution and reduced structure-function correlation. The prefrontal stimulation also modified dynamic connectivity arrangements typically associated with consciousness and unconsciousness. Our findings offer compelling evidence that PFC tDCS induces striking modifications in the fMRI-based dynamic organization of the brain across different states of consciousness. This study contributes to an enhanced understanding of tDCS neuromodulation mechanisms and has important clinical implications for disorders of consciousness.

Main Text

Introduction

At rest, the spontaneous activity of the awake brain is highly structured. The brain dynamically transitions through various resting-state functional magnetic resonance imaging (rs-fMRI) patterns, which are thought to support specific cognitive functions (Baker et al., 2014; Calhoun et al., 2014; Damoiseaux et al., 2006; Deco et al., 2013, 2011; Fox et al., 2006; Preti et al., 2017; Raichle et al., 2001; Vincent et al., 2006). Interestingly, in non-human primates (NHPs), wakefulness and unconsciousness induced by different anesthetics are associated with strikingly different sequences and occurrences of transient brain patterns (Barttfeld et al., 2015; Uhrig et al., 2018). The conscious brain is traversed by a diverse and mobile set of functional brain patterns that deviate from anatomical connectivity. In contrast, the unconscious brain is characterized by transient functional patterns that are less diverse, stiffer, and more closely follow anatomical connectivity. Similar dynamic functional configurations are found in awake and sedated humans and generalize to other contexts of loss of consciousness, whether in patients with impaired consciousness or during sleep (Castro et al., 2023; Demertzi et al., 2019; Golkowski et al., 2019; Huang et al., 2020; Luppi et al., 2021). Ultimately, these different structure-function configurations are proposed as signatures of consciousness and unconsciousness, respectively.

Over the past twenty years, transcranial direct current stimulation (tDCS) has emerged as a popular non-invasive tool for clinicians and researchers to modulate brain activity (Lefaucheur et al., 2017; Narmashiri and Akbari, 2023). Two or more electrodes are attached to the subject's head, and a weak current is applied between them, producing an electric field, part of which crosses the skull and influences the activity of underlying neurons (Lefaucheur and Wendling, 2019). While conventional tDCS relies on the use of relatively large rectangular pad electrodes, high-density tDCS (HD-tDCS) utilizes more compact ring electrodes, allowing for increased focality, stronger electric fields, and presumably, greater neurophysiological changes (Datta et al., 2009; Dmochowski et al., 2011). In vivo and in vitro data suggest that tDCS acts through diverse, concurrent, and multiscale modes of action (Lefaucheur et al., 2017; Lefaucheur and Wendling, 2019). Importantly, ongoing neural activity during tDCS administration is likely to be critical, as tDCS effects are state-dependent and primarily modulate active networks (Antal et al., 2007; Bikson et al., 2013; Li et al., 2019).

Recent studies suggest that tDCS may influence the level of consciousness. Anodal tDCS of the left dorsolateral prefrontal cortex (DLPFC) improves signs of consciousness in patients with disorders of consciousness (DOCs) (Angelakis et al., 2014; Hermann et al., 2020; Liu et al., 2023; Thibaut et al., 2014) and can increase rs-fMRI connectivity in some of these patients, both at the site of stimulation and in remote regions (Peng et al., 2022). However, the effects of PFC tDCS on resting-state dynamic brain patterns typically associated with consciousness have never been investigated. In healthy humans, tDCS can perturb both occurrences and transitions of some rs-fMRI co-activation patterns (CAPs) (using the DLPFC as a seed), suggesting that some elements of brain dynamics could be affected by tDCS in the awake resting brain. The effects of tDCS on brain activity during anesthesia-induced loss of consciousness remain largely unexplored. Repeated stimulation of the rat motor cortex facilitates the return of the righting reflex and visual and working memory after isoflurane anesthesia (Mansouri and García, 2021), suggesting that tDCS may represent a novel approach to accelerate recovery from general anesthesia (Kato and Solt, 2021).

However, these studies left many questions unanswered. Does PFC tDCS possess the ability to remodel the functional and structural brain organization characteristic of the conscious and unconscious brain? For example, can it affect the order and relative frequency of fMRI brain connectivity patterns, as well as other aspects of brain dynamics, such as the structure-function correlation and the Shannon entropy (Demertzi et al., 2019)? If so, do the polarity (e.g., anodal versus cathodal), the intensity (e.g., 1 mA versus 2 mA), and the timing of the stimulation (e.g., during versus after the stimulation) perturb these metrics differently? Ultimately, does tDCS have enough perturbational power to affect the dynamic configurations of connectivity characteristic of consciousness and unconsciousness residing in cortical brain dynamics? Answering these questions may both advance our comprehension of the neural mechanisms underlying tDCS effects and provide meaningful information for clinicians.

This study aimed to determine whether HD-tDCS targeting the PFC can modify the relationship between the structural and functional brain organization in fMRI signals in NHPs, either in the awake state or under deep propofol anesthesia. Our specific aims were to determine the effects of PFC HD-tDCS on brain dynamics 1) in awake NHPs receiving either anodal or cathodal stimulation, 2) in deeply anesthetized NHPs receiving anodal stimulation at two different intensities, and 3) the time course of these putative changes relative to the stimulation (i.e., during and after the stimulation). Our results provide evidence that anodal prefrontal HD-tDCS only marginally affected the brain dynamics in awake animals. In contrast, cathodal prefrontal HD-tDCS significantly reorganized the functional repertoire in favor of anatomically similar brain patterns without apparent behavioral modification. Moreover, both anodal and cathodal stimulation affected Markov chain transitions between brain patterns, with some changes specific to ongoing stimulation and others to post-stimulation. Under anesthesia, anodal prefrontal HD-tDCS delivered at an intensity of 2 mA, but not 1 mA, significantly reduced the structure-function correlation but did not fully restore the broad and rich dynamic repertoire of functional patterns characteristic of wakefulness, nor did it induce signs of arousal in the animals. Altogether, these findings illustrate the ability of tDCS to modulate conscious and unconscious brain dynamics in a polarity- and intensity-dependent manner.

Results

We established an experimental procedure that allowed HD-tDCS and fMRI data acquisition from macaque monkeys (*Macaca mulatta*) in two states of consciousness: awake and under general anesthesia (Figure 1). To characterize the functional and structural brain organization in fMRI signals and how they are affected by the stimulation, we calculated the dynamic functional connectivity between 82 cortical regions of interest (ROIs) based on the CoCoMac anatomical database. We used the Hilbert transform to estimate the phase of fMRI signals at each TR and computed the coordination between the continuous fMRI time series across all ROIs. We then

applied the unsupervised K-means algorithm to cluster the phase-based coherence matrices. This allowed for the identification of recurrent patterns of brain connectivity. Finally, we sorted the brain patterns based on their degree of similarity to the CoCoMac anatomical matrix and calculated the relative occurrence rates of the patterns, the structure-function correlation (SFC), and the Shannon entropy for each vigilance state, electrode arrangement, and stimulation condition.

In Figures 3-6, we present the results for brain patterns (or *k* clusters) fixed to 6, as this number was determined to be the best choice for maximizing the inter-pattern correlation variance (IPCV) when considering awake and anesthesia datasets together (Figure 2). Additionally, we verified that varying the number of brain patterns (or *k* clusters) in the K-means algorithm from 3 to 10 did not change the principal findings in the paper (Figure 2 - figure supplements 1-3). Boxplots displaying the main measurables (slope's coefficient and Shannon entropy) as a function of said *k*-number of clusters were also done (figure supplement 1 of Figures 3, 5, 6 & 7) to further demonstrate the consistency of our results, regardless of the choice of *k*.

Polarity-dependent effects of prefrontal HD-tDCS on the cortical dynamic connectivity in awake macaques

To examine whether HD-tDCS can perturb the repertoire of functional connectivity patterns characteristic of the awake state, we collected a total of 288 fMRI runs before, during, and after the application of HD-tDCS at an intensity of 2 mA in two macaque monkeys using two different electrode setups (Figure 1A).

The dynamic connectivity analysis was performed on data from all five awake experimental conditions: before HD-tDCS, during HD-tDCS using anodal or cathodal montages, and after anodal or cathodal HD-tDCS (Figure 3). The resulting patterns exhibited a variety of complex configurations of interregional connectivity. These included long-range positive/negative coherences (patterns 1 and 3), mostly frontal positive and parieto-occipital negative coherences (patterns 2 and 4), and almost strictly positive medium or low interregional coherences (patterns 5 and 6) (Figure 3A). We then calculated the probability distribution of the occurrence of each pattern across the stimulation conditions (Figure 3C). Brain pattern 6, referred to as the 'anatomical pattern' due to its highest correlation with the CoCoMac connectome, showed the most numerous and strongest differences in visit frequency. The time spent in this pattern increased sharply during and following stimulation with the cathodal montage compared to before stimulation and to the corresponding conditions with the anodal montage. This later finding shows the specificity of the effects of the cathodal stimulation. The time spent in brain state 5 was markedly shorter in the cathodal post-stimulation condition compared to pre-stimulation. Cathodal stimulation also shortened the time spent in brain state 3 during stimulation compared to the corresponding condition with the anodal montage. In sharp contrast, the distribution of pattern occupancies during or following stimulation with the anodal montage did not exhibit much change compared to pre-stimulation. These polarity-specific effects of prefrontal HD-tDCS were further illustrated by plotting the occurrence rate per condition (Figure 3D). These results suggest that the cathodal stimulation lowered the occurrence of patterns with high frontal coherence (patterns 1, 3, and 5), but promoted the visit of patterns with predominant parieto-occipital coherence (patterns 2 and 4) or very low coherence (pattern 6). All significant statistics are shown in Table 4A. It should be noted that these alterations of brain dynamics were not accompanied by any obvious behavioral changes in the monkeys, as they continued to show consistent and optimal eye fixation rates (Table 2).

Next, we computed the Shannon entropy from the normalized histograms of occurrences (Figure 3E, Table 4A). The Shannon entropy was considerably lower during and after cathodal stimulation compared to before stimulation and during cathodal stimulation compared to during anodal stimulation. In contrast, the Shannon entropy was not affected by stimulation with the anodal montage, further supporting the polarity-dependent nature of the effects. This result implies that cathodal, but not anodal stimulation limits the degree of surprise held in the distribution of pattern rates. A lower Shannon entropy was reported in many different studies investigating anesthesia-

induced loss of consciousness in humans (Castro et al., 2023; Golkowski et al., 2019), in macaques (Barttfeld et al., 2015; Uhrig et al., 2018), under sleep-induced loss of consciousness in humans (Castro et al., 2023; Patel et al., 2020), and in patients suffering from disorders of consciousness (Demertzi et al., 2019). Moreover, recovery from general anesthesia in humans (Castro et al., 2023; Patel et al., 2020) and restoration of arousal and wakefulness in anesthetized macaques by deep brain stimulation of the central thalamus (Luppi et al., 2024; Tasserie et al., 2022) were both associated with recovery of a higher Shannon entropy value.

We then evaluated the relationship between the centroids' presence rate and the anatomical backbone in monkeys. We plotted the presence rates of all the centroids, for all macaques, as a function of their SFC. Considering the averages of occurrence rates over the different conditions, we computed one linear regression (per condition), to show the overall linear relationship between the time spent in the various brain states and their similarity to the anatomical connectivity for each condition (Figure 3F). We then repeated such computation but for all subjects and all conditions (Figure 3G), and performed statistics on these distributions (shown in Table 4A*)*. The slope was substantially heightened during and after stimulation with the cathodal montage compared to before stimulation. In addition, during stimulation and post-stimulation, the cathodal montage was associated with a significantly higher slope coefficient compared to the anodal montage. Consistent with our previous observations, the stimulation with the anodal montage had a negligible influence on this metric compared to the pre-stimulation condition. These results were not affected by the choice of the number of *k* clusters (Figure 3 - figure supplement 1), and similar results were obtained when the full analysis was repeated for *k* = 4 (Figure 3 - figure supplement 2), as suggested by the IPVC (Figure 2).

Next, we analyzed the succession of brain states through the prism of a Markov chain. Both anodal and cathodal stimulations produced significant changes in probability transitions (Figure 4). The corresponding statistics are shown in Table 4B. Strikingly, cathodal stimulation induced much greater transition probabilities from brain states 1 and 2 to brain state 6 (Figure 4A). Conversely, transitions from brain states 2 to 3, from 5 to 2, and 6 to 5 were significantly reduced by cathodal stimulation. Other changes were observed only after cathodal stimulation, including an increase in the probability of transitioning from brain states 5 to 6 and a probability decrease of transitioning from states 6 to 3. Ultimately, cathodal PFC HD-tDCS strongly promoted transitions to brain state 6 and weakly inhibited some transitions leaving this state. As for anodal stimulation, it significantly favored the transitions from brain states 3 to 5 and from 2 to 3, and reduced the transitions from brain states 2 to 4 and 1 to 5 (Figure 4B). While these effects weren't sustained post-stimulation, the transition from brain states 2 to 6 was significantly perturbed post-stimulation. Overall, anodal PFC HD-tDCS weakly altered only a few transitions. Our results also show that the Markov chain transition probabilities are affected differently during and after HD-tDCS. Some changes were observed only during ongoing current delivery, while others were specific to the post-stimulation condition. Importantly, the fact that both categories of changes were found in cathodal and anodal experiments suggests a general phenomenon.

Contrasting the effects of prefrontal HD-tDCS on the dynamic connectivity patterns in wakeful macaques to unconscious dynamics

Dynamic connectivity configurations associated with consciousness have previously been identified by analyzing data from conscious and unconscious states together (Barttfeld et al., 2015; Castro et al., 2023; "Conscious Processing and the Global Neuronal Workspace Hypothesis," 2020; Demertzi et al., 2019; Uhrig et al., 2018). We therefore repeated our analysis of the data from all five awake experimental conditions pooled with the anesthesia pre-stimulation condition (Figure 5). All significant statistics are shown in Table 4C.

The six resulting brain patterns showed somewhat different trends in connectivity arrangements compared to the patterns that emerged from the analysis of the awake data alone. While patterns 1 and 2 closely matched the previously obtained awake patterns 1 and 2, the others showed distinct

connectivity configurations (Figure 5A). As expected, both the awake and the anesthesia pre-stimulation conditions exhibited significant differences in the rates at which the six brain patterns occurred (Figure 5C,D). Pattern 1 was present in the awake pre-stimulation condition but virtually absent in the anesthesia pre-stimulation condition, whereas patterns 5 and 6 were predominant under anesthesia. These findings are consistent with previous dynamic rs-fMRI studies in macaques and humans (Barttfeld et al., 2015; Demertzi et al., 2019; Uhrig et al., 2018). The cathodal montage again produced strong perturbation effects. Compared to pre-stimulation, state 4, characterized by short-range frontal coherences, occurred for a significantly shorter time during and after stimulation. State 6, the so-called anatomical pattern, showed differences between conditions, consistent with our previous analysis of the awake conditions. As previously observed, cathodal HD-tDCS increased the occurrence rate of state 6, while anodal stimulation had no effect. Therefore, consistent with the prior analysis of the data taken from the awake conditions alone, the cathodal stimulation reduced the incidence of the pattern with a predominant frontal coherence (here, pattern 4), while it increased the incidence of the 'anatomical' pattern (pattern 6).

The Shannon entropy was found to be much lower in anesthetized monkeys than in awake animals (Figure 5E). This finding is consistent with previous studies in humans, regardless of whether unconsciousness was due to disorders of consciousness, deep sleep, or anesthesia (Castro et al., 2023; Demertzi et al., 2019). While anodal stimulation had no effect, prefrontal cathodal stimulation significantly diminished Shannon entropy, similar to the previous analysis (Figure 3E). Consistent with our previous results, the cathodal HD-tDCS induced a direct and lasting effect that was captured in our SFC-frequency analysis, where the states with high SFC were more present compared to those with low SFC (Figure 5F,G). These perturbations were noticeable when considering each macaque, and the effects observed during and post-cathodal stimulation were strong enough to alter the slopes. Compared to pre-stimulation, the changes observed during and post-stimulation were significant and had a similar tendency: an increase in the SFC-slope's coefficient. Finally, these differences were specific to the cathodal montage, and the comparison between the two types of electrode arrangements again revealed statistically significant differences. These results remained robust regardless of the number of *k* clusters (Figure 5 - figure supplement 1).

Effects of prefrontal HD-tDCS on the dynamic connectivity patterns in anesthetized macaques

Under propofol anesthesia, we adopted a slightly different experimental design, as we aimed to determine the effects of anodal HD-tDCS of the PFC with increasing intensity. We acquired fMRI data before, during, and after HD-tDCS delivered at an intensity of 1 mA, followed by a second block of stimulation at 2 mA (Figure 1B). A total of 136 runs were acquired in two macaque monkeys. We also continuously monitored vital parameters related to hemodynamics, ventilation, and temperature (Table 3). The dynamic signal coordination analysis was applied to the collected data. All significant statistics are shown in Table 4D.

Compared to the patterns observed from the analysis of the awake conditions alone (Figure 3A), the patterns generated from this experimental setup showed different organizations of interconnectivity between regions, with patterns 2, 3, 4, and 5 displaying primarily frontal/prefrontal coherences (Figure 6A). Interestingly, in the 2 mA post-stimulation condition, brain states 2 and 5 presented an increase in their presence rates compared to pre-stimulation, while brain state 6 showed a decrease (Figure 6C). Plotting the frequency of pattern visits across conditions further illustrated the notable reduction in the prevalence of brain state 6, the higher occurrence rate of states 2 and 5, as well as a tendency for the effects of the stimulation to gradually rise as a function of stimulation intensity (Figure 6D). Comparisons of Shannon entropy were non-significant (Figure 6E). However, for the 2 mA post-stimulation condition, the slope coefficient was statistically reduced compared to pre-stimulation (Figure 6F,G). These results remained robust regardless of the number of *k* clusters (Figure 6 - figure supplement 1).

Because the IPVC suggested that 9 brain patterns would be optimal to reach the maximum IPVC for the anesthesia dataset (Figure 2), we repeated the complete analysis for *k*=9 (Figure 6 - figure supplement 2). Using *k*=9, we found even more perturbations in brain dynamics by HD-tDCS than with *k*=6. Firstly, the 'anatomical' brain state's occurrence rate was significantly lower both during and following 2 mA stimulation. Additionally, brain states 5 and 8 (which resemble brain states 2 and 5 in the analysis with *k*=6 in Figure 6A) showed an increase in their occurrence during and following stimulation at 2 mA. Finally, the slope coefficient was significantly decreased during and after 2 mA stimulation compared to before. No effect on the Shannon entropy was observed.

Next, we contrasted the data from all anesthesia conditions with the awake pre-stimulation condition, keeping k=6 for the k-means clustering (Figure 7). As expected, all the patterns except pattern 5 showed significantly different occurrence rates between the awake and anesthesia pre-stimulation conditions (Figure 7C), consistent with the previous contrasted analysis (Figure 5C) and the literature (Barttfeld et al., 2015; Demertzi et al., 2019; Uhrig et al., 2018). Compared to pre-stimulation, brain state 3, a high positive frontal coherence pattern, was visited more often, and brain state 6 less frequently in the 2 mA post-stimulation condition. The slope coefficient was statistically reduced compared to pre-stimulation (Figure 7G), regardless of the number of *k* clusters (Figure 7 - figure supplement 1). These results show that 2 mA anodal PFC stimulation can reconfigure unconscious brain dynamics under anesthesia, albeit it could not restore the full range of characteristics of awake cortical dynamics, such as the visit of brain pattern 1. In line with these findings, these modulations were not accompanied by any behavioral signs of awakening in the animals. Nevertheless, the stimulation did influence some vital parameters (heart rate, systolic and diastolic blood pressure) (Table 3), as previously reported (Gu et al., 2022; Rodrigues et al., 2022).

Lastly, we studied how the Markov chain transitions between brain states across stimulation conditions under anesthesia. However, during and following stimulation, at both 1 and 2 mA, not a single transition passed the bootstrapping method, even when the confidence level was reduced to 90%. Thus, we could not interpret any possible changes in transition probability since those empirical transitions can't be considered specific nor temporally independent. As such, we do not show this analysis.

Discussion

The dynamic nature of brain activity and connectivity in resting-state fMRI has attracted considerable interest over the past years. In this study, we demonstrate that tDCS perturbs dynamic brain patterns in awake but also deeply sedated macaques. We also show that the dynamic cortical connectivity arrangements previously described to typify consciousness and unconsciousness can be non-invasively influenced by a weak direct current applied transcranially. Our findings are consistent with the hypothesis that tDCS directly affects brain dynamics. In the following, we discuss the implications and potential mechanisms associated with the dynamic changes induced by tDCS.

Cathodal prefrontal HD-tDCS strongly perturbed cortical brain dynamics in awake macaques

In awake animals, our analysis showed that cathodal stimulation of the PFC markedly alters the relative prevalence of cortical signal coordination patterns (Figures 3 and 5). We found that the 'anatomical' pattern (pattern 6) was the most sensitive to cathodal stimulation. Our observations that the prevalence of this pattern and the transitions towards it are greatly enhanced by cathodal stimulation in a conscious wakeful context are both unexpected and surprising. One explanation might be that this pattern is related to transient drops in vigilance levels and that cathodal stimulation might enhance such a phenomenon. Contamination of fMRI data by transient periods of microsleep has been shown to occur frequently in awake resting-state experiments (Tagliazucchi and Laufs, 2014). Interestingly, some recent papers suggested that tDCS over prefrontal or frontal

regions can influence arousal, sleepiness, or sleep quality (Annarumma et al., 2018; Frase et al., 2016). For instance, cathodal bi-frontal tDCS delivered immediately before sleep has been found to increase total sleep time and decrease cortical arousal in healthy volunteers (Frase et al., 2016). However, in our experiments, the stimulated animals showed no tendency to drowsiness or any sudden restlessness in an attempt to resist sleep. Furthermore, the animals were not resting but engaged in a fixation task throughout the fMRI data acquisition. It is also worth noting that they completed the task with a similar success rate in the cathodal stimulation condition compared to the pre-stimulation or anodal stimulation conditions (Table 2). Therefore, our observations do not seem to be compatible with an increase in drowsiness or a reduction in vigilance due to cathodal stimulation.

Alternatively, other types of mental processes might be enhanced by cathodal tDCS, such as the tendency to mind-wander, to experience mind-blanking, or to enter a hypnotic state. A seminal study showed that anodal prefrontal cortex stimulation can significantly boost the tendency to mind wander in healthy adults (Axelrod et al., 2015). However, subsequent efforts to replicate these findings yielded conflicting results (Coulborn and Fernández-Espejo, 2022; Nawani et al., 2023). Mind-blanking is a state where the mind is alert but not actively engaged in a specific cognitive task. Reports of mind-blanking were recently found to correlate with a pattern of global positive-phase coherence rather than the pattern that most closely resembles anatomy (Mortaheb et al., 2022). This finding does not support an enhancement of mind-blanking by cathodal stimulation of the PFC in our study.

Finally, cathodal left DLPFC tDCS was demonstrated to enhance hypnotizability by 15% and to alter some dimensions of consciousness, significantly increasing attention, absorption, and time sense but decreasing self-awareness and memory (Perri et al., 2022; Perri and Di Filippo, 2023). While our observations of the monkey's high fixation task performance would be consistent with increased attention or absorption, the demonstration of a modulatory effect of cathodal tDCS on one or other of these specific mental processes or dimensions of consciousness will require further investigation in humans using relevant behavioral measures, cognitive tasks, and brain activity tracking.

Anodal prefrontal HD-tDCS perturbed cortical brain dynamics, especially during deep anesthesia.

In awake macaques, we found that the anodal montage significantly disturbed some transition probabilities between brain states (Figure 4C,D). Anodal stimulation tended to decrease the slope's coefficient (Figures 3G and 5G) and to increase the occurrence rate of brain state 1 (Figures 3C,D and 5C,D). Although small, these changes are consistent with recent literature suggesting that anodal PFC tDCS, when delivered during the daytime, can positively influence levels of vigilance and sleepiness (Annarumma et al., 2018). For example, this type of stimulation has been described to increase beta and decrease delta powers in a wakeful context, thus indicating enhanced vigilance (Dai et al., 2022; Maeoka et al., 2012; Wirth et al., 2011). Bifrontal anodal stimulation increased objective and subjective vigilance and reduced daytime sleepiness in a patient with organic hyperinsomnia following reanimation (Frase et al., 2015). Moreover, in sleep-deprived adults, bifrontal anodal tDCS also reduced EEG correlates of physiological sleepiness (Alfonsi et al., 2023). Anodal left DLPFC tDCS performed better than caffeine in preventing the reduction in vigilance and alleviating subjective ratings of fatigue and drowsiness in sleep-deprived individuals (McIntire et al., 2014). Finally, such a stimulation affected total sleep time, shortening it by about 25 min, when administered just before sleep in healthy volunteers (Frase et al., 2016).

While we observed modest effects of anodal PFC HD-tDCS in awake animals, the stimulation produced significant changes in cortical brain dynamics under anesthesia and reduced the structure-function correlation, suggesting a kind of in-between state between wakefulness and anesthesia (Figures 6 and 7). Therefore, although our protocol did not succeed in awakening the sedated animals, our results support the ability of prefrontal tDCS to affect brain dynamic patterns related to consciousness in the context of an anesthesia-induced loss of consciousness. It can be

hypothesized that the molecular effect of the anesthetic drug was stronger than the electrical effect at an intensity of 2 mA, which could explain the lack of behavioral effects. However, it remains possible that a similar protocol could succeed in awakening macaques sedated with a lower dose of propofol or in reversing unconsciousness due to deep propofol anesthesia with a higher stimulation intensity. In this case, the effects may reach a threshold where we get as much disturbance from pharmacology as physical intervention, thus resulting in an observable behavioral effect of tDCS. This idea is supported by the fact that we observed a greater effect on brain dynamics at 2 mA compared to 1 mA. Interestingly, a recent study in humans showed that tDCS delivered at 4 mA intensity can robustly enhance the effects of stimulation compared to 2 mA and is safe, well-tolerated, and without adverse effects (Hsu et al., 2023; Nitsche and Bikson, 2017). Therefore, our results encourage further investigation using anodal prefrontal HD-tDCS at an intensity of 4 mA to non-invasively attempt to reverse the effects of deep propofol anesthesia. Our findings also support the use of tDCS to promote rapid recovery from general anesthesia in humans (Kato and Solt, 2021) and suggest that a single anodal prefrontal stimulation at the end of the anesthesia protocol may be effective.

From another clinical perspective, our results demonstrating that 2 mA anodal PFC tDCS decreased the structure-function correlation and modified the dynamic repertoire of brain patterns during anesthesia (Figures 6 and 7) are consistent with the beneficial effects of such stimulation in DOCs patients (Angelakis et al., 2014; Thibaut et al., 2014). For instance, a recent meta-analysis has concluded that tDCS is more effective in improving the level of consciousness in patients with a minimally conscious state (MCS) than in those with an unresponsive wakefulness syndrome (UWS), which is a more severe form of this medical condition (Liu et al., 2023). Our results support the efficacy of tDCS in improving consciousness markers in patients with DOCs, particularly in the least severely affected patients, and encourage the design of new clinical trials to investigate the effects of higher stimulation intensities.

From a mechanistic point of view, prefrontal tDCS may modulate arousal and improve the level of consciousness by acting on the recently proposed cortico-thalamic pathway of sleep-wake regulation or by acting directly on the ascending thalamocortical pathway, which originates in the brainstem (Krone et al., 2017). Depending on electrode positions and stimulation parameters, tDCS has been shown to modulate subcortical regions directly. For example, fronto-temporal tDCS has been reported to alter corticostriatal and corticothalamic rs-fMRI connectivity in healthy volunteers (Dalong et al., 2020; Polanía et al., 2012). In vivo measurements in humans using intracerebral electrodes confirmed that the stimulation can generate a biologically relevant electric field at the subthalamic level or other deep brain structures (Guidetti et al., 2022; Louviot et al., 2022). Computational modelling of the electric field (Huang et al., 2012; Saturnino et al., 2019) generated by the specific fronto-occipital montage used in this study will likely yield valuable information regarding which pathway (cortico-thalamic or thalamocortical) may have been modulated. Furthermore, modulation of intrinsic networks (Boly et al., 2008; Raichle et al., 2001) is possible in light of our result and could also be investigated through an iCAPs-based analysis (Ensel et al., 2023; Karahanoğlu and Van De Ville, 2015).

From a biophysical standpoint, previous studies showed that anodal stimulation leads to depolarization at the soma of neurons in rat hippocampal slices, while cathodal stimulation induces their hyperpolarization, especially when the current is aligned with the soma-apical axis (Bikson et al., 2004). These findings were corroborated in human subjects (Nitsche and Paulus, 2000), where anodal tDCS applied to the motor cortex increased the amplitude of motor-evoked potentials in response to transcranial magnetic stimulation, while cathodal M1 stimulation had the opposite effects, revealing an increase or decrease in M1 excitability, respectively. The magnitude of these effects was small (0.2 mV) (Bikson et al., 2004) but fell within the range of endogenous electric field interactions generated between cortical columns, where it can be greatly amplified by recurrent interactions (Rebollo et al., 2021). Interestingly, in the awake state, we observed that cathodal stimulation of the PFC induced a significant decrease in the frequencies of patterns exhibiting high frontal coherence (patterns 3 and 5), which is consistent with a reduction in PFC excitability under

the cathodal electrode. In contrast, the stimulation with this montage tended to increase the frequency of patterns with a predominant parieto-occipital coherence (patterns 2 and 4), which is in line with an increase in excitability under the anodal electrode positioned over the occipital cortex (Figure 3A,C). Under anesthesia, 2 mA anodal HD-tDCS of the PFC increased the frequencies of some patterns exhibiting a high frontal coherence (patterns 2 and 5) (Figure 6A,C), also supporting enhanced excitability under the anodal electrode in deep sedation. It is important to note that the effects of the neuromodulatory ascending systems on brain activation are known to be mediated both by neuronal depolarization and by inhibition of voltage and calcium-dependent conductance, which are responsible for spike-frequency adaptation in pyramidal cells (McCormick, 1992; Steriade and McCarley, 2013). Therefore, one possible explanation for the inability of anodal stimulation of the PFC to arouse macaques from anesthesia is that it caused depolarization of neurons without affecting spike-frequency adaptation and thus only partially activated the brain.

Markov chain analysis revealed differential HD-tDCS effects on transition probabilities during and after stimulation

Our results showed relatively similar effects during and after the stimulation in terms of brain pattern occurrence rates, Shannon entropy, and SFC (Figures 3, 5, 6, 7). In contrast, Markov chain analysis revealed the existence of specific changes in transition probability induced by HD-tDCS, some of which were found only during stimulation and others exclusively in the post-stimulation condition (Figure 4, Table 4B). Our results highlight that certain effects of HD-tDCS on brain dynamics are specific to the time course of the stimulation and can be revealed using particular dynamic analyses such as the Markov chain transition.

In conclusion, our data provides experimental evidence that HD-tDCS of the prefrontal cortex modulates spontaneous brain activity whether the animals are wakeful and conscious, or unconscious under general anesthesia. Our study offers a deeper understanding of how tDCS influences and alters brain dynamics, which is crucial given its growing applications in neuroscience and the management of various neurological conditions. Finally, our work suggests that by allowing a soft, non-invasive and reversible perturbation of brain activity, tDCS may be a valuable tool for further investigations of the relationship between brain dynamics and states of consciousness, conscious processing, or vigilance.

Materials and Methods

Animals

Four rhesus monkeys (*Macaca mulatta*, 18-20 years, 7.2-9.8 kg) were scanned. Two males were tested for the awake experiments (monkeys J and Y), and one female and one male were tested for experiments under anesthesia (monkeys R and N). All procedures followed the European Convention for Animal Care (86-406) and the National Institutes of Health's Guide for the Care and Use of Laboratory Animals. Animal studies were approved by the Institutional Ethical Committee (CETEA protocol #16-040).

Transcranial Direct Current Stimulation

We applied HD-tDCS using a battery-powered stimulator (1x1 tES device, Soterix medical) located outside the scanner room and a complete MR-compatible setup consisting of an MRI filter, carbon composition cables, and two high-density (HD) carbon rubber electrodes inserted into HD-tES MRI electrode holders (Soterix medical). The electrode setups and experimental designs used in awake and anesthetized macaques are shown in Figure 1.

Electrode contact quality was checked before all stimulation sessions using the device's Pre-stim Tickle function (1 mA for 30 s). If a poor contact was detected, the electrode-scalp contact was readjusted, and conductive paste or gel was added to improve contact quality. Electrode contact quality was continuously monitored during the stimulation.

To reduce the likelihood of the monkeys experiencing discomfort at the electrode sites, the current was gradually increased from 0 mA to the target intensity over the first 30 seconds. The current was also gradually decreased to 0 mA over the last 30 seconds of each tDCS stimulation period. The tDCS device was turned off during the acquisition of the pre- and post-stimulation fMRI blocks to avoid any hypothetical biological effect of the residual current (Fonteneau et al., 2019), which we measured to be 0.023 mA. After the tDCS-fMRI scanning sessions, the monkeys' scalps were examined for redness, skin burns, or other lesions. None of the monkeys showed any side effects.

Awake experiments

In the awake experiments, elastic bands with fasteners were used to secure the electrode holders. We used a conductive and adhesive paste (Ten20 conductive paste, Weaver and Company) to ensure consistent electrode-skin contact. The anode electrode was placed over the left PFC (F3) and the cathode electrode over the right occipital cortex (O2), or the reverse montage was employed, with the cathodal electrode placed over the right PFC (F4) and the anode over the left occipital cortex (O1). We used monkey EEG caps (EasyCap, 13 channels, Fp1, Fp2, F3, F4, T3, T4, P3, P4, O1, O2, Oz, reference electrode, ground electrode), based on the international 10-20 EEG system, to obtain F3, F4, O1, and O2 locations, where we placed the stimulation electrodes. The two montages were respectively abbreviated F4/O1 and O1/F4. tDCS was delivered for 20 min at a current intensity of 2 mA.

Anesthesia experiments

For anesthesia experiments, the electrode holders were held in place with Monkey-2D caps (EasyCaps GmbH), using an EEG gel to obtain low impedance (One Step EEG gel, Germany) as the conductive medium. Monkey R was stimulated with an F3/O2 montage (anodal electrode over the left PFC and cathodal electrode over the right occipital cortex) and monkey N was stimulated with an F4/O1 montage (anodal electrode over the right PFC and cathodal electrode over the left occipital cortex). This different but still close placement of the electrodes between the two animals was dictated by constraints related to the location of the headpost (with the cement used to anchor the headpost spreading more or less asymmetrically) and the anatomy/specificity of each animal's head. Because of the small size of the monkey's head, we expected that tDCS stimulation with these two symmetrical montages would result in nearly equivalent electric fields across the monkey’s head and produce roughly similar effects on brain activity. Two 20-minute blocks of tDCS stimulation were applied consecutively in each scanning session, with a current intensity of 1 mA for the first block and 2 mA for the second block (Figure 1).

<u>fMRI Data Acquisition</u>

The monkeys were scanned on a 3-T horizontal scanner (Siemens Prisma Fit, Erlanger, Germany) with a custom-built single transmit-receiver surface coil. The parameters of the fMRI sequences were as follows: (i) functional scan: EPI, TR = 2400 ms, TE = 20 ms, 1.5-mm isotropic voxel size, and 111 brain volumes per run, (ii) anatomical scan: MPRAGE, T1-weighted, TR = 2200 ms, TE = 3,18 ms, 0.80-mm isotropic voxel size, sagittal orientation. Before each scanning session, monocrystalline iron oxide nanoparticles (10 mg/kg, i.v.; MION, Feraheme, AMAG

Pharmaceuticals, MA) were injected into the saphenous vein of the monkey to improve the contrast-to-noise ratio and the spatial selectivity of the MR signal changes (Vanduffel et al., 2001).

All fMRI data were acquired while the monkeys were engaged in a passive event-related auditory task, the local-global paradigm, based on local and global deviations from temporal regularities (Bekinschtein et al., 2009; Uhrig et al., 2014). The investigation of how tDCS perturbs cerebral responses to local and global deviants will be analyzed later and is not shown in this paper. fMRI data were acquired before tDCS stimulation, during tDCS stimulation (onset of fMRI acquisition starting after the ramp-up period and stopping before the ramp-down period), and after tDCS stimulation. For anesthesia experiments, a second round of stimulation/post-stimulation block was completed (see below). Four runs of 111 brain volumes were acquired during each condition (before tDCS stimulation, during tDCS stimulation, and after tDCS stimulation). Finally, all sessions ended up with an anatomical scan.

Awake protocol

Monkeys were implanted with an MR-compatible headpost, trained to sit in a sphinx position in a primate chair, and to fixate within a 2×2° window centred on a red dot (0.35×0.35°) within a "mock" MR bore before being scanned. fMRI data were acquired in awake macaques as previously described (Uhrig et al., 2014). The eye position was monitored at 120 Hz (Iscan Inc., MA, USA) and the fixation rate during the fMRI run was recorded (Table 2). No physiological parameters were recorded in the awake state.

A total of 288 runs were acquired in the awake state: 136 runs before stimulation, 56 runs during anodal stimulation, 56 runs after anodal stimulation, 20 runs during cathodal stimulation, and 20 runs after cathodal stimulation (Table 1 for details of the number of runs acquired per monkey).

Anesthesia protocol

The anesthesia protocol is described in detail in a previous study (Tasserie et al., 2022). Anesthesia was induced with an intramuscular injection of ketamine (10mg/kg, Virbac, France) and dexmedetomidine (20 microgr/kg, Ovion Pharma, USA) and maintained with a target-controlled infusion (TCI) (Alaris PK Syringe pump, CareFusion, CA, USA) of propofol (Panpharma Fresenius Kabi, France) using the "Paedfusor" pharmacokinetic model (Absalom and Kenny, 2005;) (Monkey R: TCI 5.8 micrgr/ml, Monkey N: TCI 4.3 micrgr/m). Monkeys were intubated and mechanically ventilated. The physiological parameters (heart rate, noninvasive blood pressure, oxygen saturation, respiratory rate, end-tidal carbon dioxide, and skin temperature) were monitored (Maglife, Schiller, France) and recorded (Table 3). A muscle-blocking agent (cisatracurium, GlaxoSmithKline, France, 0.15 mg/kg, bolus i.v., followed by a continuous infusion rate of 0.18mg/kg/h) was used during all anesthesia fMRI sessions to avoid artifacts.

We referred to a clinical arousal scale at the beginning and end of each scanning session to characterize the behavior of monkeys in experiments under anesthesia. This scale comprises several indicators: an exploration of the environment, spontaneous movements, shaking/prodding, toe pinch, eye-opening, and corneal reflex (for more details, see (Tasserie et al., 2022; Uhrig et al., 2016).

A total of 136 runs were acquired under anesthesia: 40 runs before stimulation, 24 runs during 1 mA anodal stimulation, 24 runs after 1 mA anodal stimulation, 24 runs during 2 mA anodal

stimulation, and 24 runs after 2 mA anodal stimulation (see Table 1 for details of the number of runs acquired per monkey).

Statistical Analysis of the Physiological Data

One-way analysis of variance (ANOVA) was used to compare the effect of the stimulation on mean heart rate, blood pressure, and other vital parameters under anesthesia (Table 3). Statistical analysis and multiple comparisons were performed using home-made MATLAB scripts (MathWorks, USA), with a statistical threshold of $p < 0.05$, Bonferroni-corrected.

fMRI Data Analyses

fMRI preprocessing

Functional images were reoriented, realigned, resampled (1 mm isotropic), smoothed (Gaussian kernel, 3 mm full width at half maximum), and rigidly co-registered to the anatomical template of the monkey MNI space (Frey et al., 2011) using custom-made scripts (Uhrig et al., 2014).

The global signal was regressed out from the images to remove any confounding effects due to physiological changes (e.g., respiratory or cardiac variations). Voxel time series were filtered with low-pass (0.05 Hz cutoff) and high-pass (0.0025 Hz cutoff) filters and a zero-phase fast Fourier notch filter (0.03 Hz) to remove an artifactual pure frequency present in all the data (Barttfeld et al., 2015; Uhrig et al., 2018).

An additional cleaning step was performed to check the data quality after time series extraction, as described previously (Signorelli et al., 2021). The procedure was based on a trial-by-trial visual inspection by an expert neuroimager of the time series for all nodes, the Fourier transform of each signal, the functional connectivity for each subject, and the dynamical connectivity computed with phase correlation. For each dataset, visual inspection was first used to become familiar with the characteristics of the entire dataset: how the amplitude spectrum, time series, FC, and dynamic FC look. Subsequently, each trial was inspected again with a particular focus on two main types of potential artefacts. The first one corresponds to potential issues with the acquisition and is given by stereotyped sinusoidal oscillatory patterns without variation. The second one refers to potential head or other movement not fully corrected by our preprocessing procedure. This last artefact can be sometimes recognized by bursts or peaks of activity. Sinusoidal activity generates artificially high functional correlation and peak of frequencies in the amplitude spectrum plot. Uncorrected movements generate peaks of activity with high functional correlation and sections of high functional correlations in the dynamical FC matrix. If we observed any of these anomalies we rejected the trial, opting to adopt a conservative policy. Trials were retained if the row signal showed no evidence of artifactual activity, the functional connectivity was coherent with the average and the dynamical connectivity showed consistent patterns over time.

Finally, a total of 295 runs were analyzed in the following conditions: awake state, 190 runs (before HD-tDCS, 82 runs; during anodal HD-tDCS, 38 runs, after anodal HD-tDCS, 39 runs, during cathodal HD-tDCS, 15 runs, after cathodal HD-tDCS, 16 runs) and anesthesia, 105 runs (before HD-tDCS, 34 runs; during 1 mA anodal HD-tDCS, 18 runs; after 1 mA anodal HD-tDCS, 18 runs; during 2 mM anodal HD-tDCS, 17 runs; after 2 mA anodal HD-tDCS, 18 runs).

Anatomical Parcellation and Structural Connectivity

Anatomical connectivity data were obtained from a recent macaque connectome generated by coupling diffusion MRI tractography with axonal tract tracing studies (Bakker et al., 2012; Shen et al., 2019). The macaque cortex was subdivided using the Regional Map parcellation method (Kötter and Wanke, 2005). The parcellation includes 82 cortical regions of interest (41 ROIs per hemisphere). Structural (i.e., anatomical) connectivity data are represented as matrices in which the 82 cortical regions of interest are plotted on the x-axis and y-axis. The CoComac connectivity matrix contains information about the strength of the connections between cortical areas, with each cell representing the connection between any two regions.

Signals Representation

Given a real-valued signal $x(t)$, there exists a unique analytic representation $\tilde{x}(t)$, which is a complex signal, with the same Fourier transform as the real-valued signal strictly defined for positive frequencies. This analytic signal can be constructed from the real-valued signal using the Hilbert transform H:

$$\tilde{x}(t) = x(t) + iH[x(t)]$$

i being the squared root of -1, the imaginary unit. The motivations for using the analytic signal are that, given some real-value data (i.e. MION signals), one can determine two functions of time that provide more meaningful properties of the signal. For a narrowband signal that can be written as an amplitude-modulated low-pass signal $A(t)$ with carrier frequency expressed by $\varphi(t)$:

$$x(t) = A(t)\cos[\varphi(t)].$$

Then, if the Fourier transforms of $A(t)$ and $\cos[\varphi(t)]$ have separate supports, the analytic signal of a narrowband signal can be rewritten as the product of two meaningful components

$$\tilde{x}(t) = A(t)e^{i\varphi(t)}.$$

Where $A(t)$ is the instantaneous amplitude, $\varphi(t)$ the instantaneous phase obtained from the Hilbert transform $H[x(t)]$.
The narrower the bandwidth of the signal of interest, the better the Hilbert transform produces an analytic signal with a meaningful envelope and phase (Glerean et al., 2012). Adopting a band-pass filtered version of the MION time series improves the separation between the phase and envelope spectra. The time series were z-scored, and subsequently, the Hilbert transform was computed to obtain the phase of each signal at each volume and each moment (TR, i.e. one-time sample).

Phase-based Dynamic Functional Coordination

A recurrent issue in fMRI studies dealing with dynamical analysis is the arbitrary choices in the time-windows length and their overlapping when capturing temporal oscillations through a sliding-window methodology (Allen et al., 2014; Barttfeld et al., 2015; Hindriks et al., 2016; Xie et al., 2019). Thus, phase-based dynamic functional coordination was preferred (Alonso Martínez et al., 2020; Cabral et al., 2017; Demertzi et al., 2019; Vohryzek et al., 2020). Analytic representations of signals

were employed to derive a phase signal corresponding to the MION time series. We computed the instantaneous phase $\varphi_n(t)$ of the signals across all regions of interest (ROI) $n \in \{1, ..., N\}$ for each repetition time (TR) $t \in \{2, \ldots, T-1\}$. The first and last repetition time (TR) of each fMRI scan were excluded due to possible signal distortions induced by the Hilbert transform (Bracewell, 2000).

The instantaneous phase was computed using Euler's formula from the analytic signal, which was then "enfolded" within the range of $-\pi$ to π, facilitating the calculation of inter-ROI phase differences. To obtain a whole-brain pattern of phase differences, the phase coherence between pairs of areas k and j at each time t, labeled $PC(k, j, t)$, was estimated using the pairwise phase coherence defined as the cosinus of the angular difference:

$$PC(k, j, t) = \cos(\varphi_k(t) - \varphi_j(t)).$$

When areas k and j have synchronized MION signals at time t, the phase coherence takes the value 1, and when areas k and j are in anti-phase at time t, their associated phase coherence is -1. All the intermediate cases lie in between the interval $[-1, 1]$. This computation was repeated for all subjects. For each subject, the resulting phase coherence was a three-dimensional tensor with dimension $N \times N \times T$, where N is the total number of regions in the parcellation (here 82 regions) and T the total number of TR in each fMRI session. One can easily see the symmetry with respect to the spatial dimensions ($PC(k, j, t) = PC(j, k, t)$). Hence, only the triangular superior parts of the phase coherence matrices were used for later computations, thus reducing the phase space's size to $\frac{N \times (N-1)}{2}$ (the diagonal was omitted) and containing the useful available information.

K-Means Clustering

To assess recurring coordination patterns among individuals in both datasets, a multistep methodology was employed. First, the scanning sessions were transformed into matrices, wherein one dimension represented instantaneous phase differences (feature space), as explained above, and the other dimension represented time. We concatenate all the vectorized triangular superior parts for all subjects at all times and from the experimental conditions, hence obtaining phase-spaces over time matrices, one for each condition. Each resulting matrix was subjected to the k-means clustering algorithm utilizing the L2 "Euclidean" distance metric. This resulted in a discrete set of k coordination patterns and their corresponding occurrence over time.

This process yielded k cluster centroids, which served as representatives of the recurring coordination patterns, accompanied by a label indicating the closest pattern for each instantaneous phase difference at every given TR.

The number of clusters was determined for a range $k = \{3, ..., 10\}$, with 100 initializations and 200 iterations each, using the 'k-means++' initialization method, respectively to respectively ensure a maximum (or minimum) value for metrics used as a proxy for choosing the optimal k-number of clusters, and for the stability in the centroids obtained. To determine the most appropriate number of clusters, we employed the inter-pattern correlation variance (IPCV) as the primary method, as

we are mainly interested in the centroids' aspect, supplemented by the elbow method for confirmation.

The IPCV is computed by vectorizing the set of centroids for a given k and calculating the variance of Pearson correlations between each pair of centroids (Demertzi et al., 2019). The optimal k, indicating the number of clusters, is determined by identifying the maximum value of this metric. To validate this optimal k, we employed the elbow method, which is typically based on the within-cluster sum of squares differences. While the elbow was not always as distinctly observable as desired, it still often coincided with the proposed *k* from the IPCV.

Structure-Function Correlation

To investigate the dependence of brain dynamics on the state of consciousness, we defined a measure of similarity between functional and structural connectivity. We resorted to a widely used group estimate of macaque anatomical connectivity provided by the CoCoMac 2.0 database. We computed the linear correlation coefficient between the entries of both matrices (k-means centroids and anatomical connectome) for each set of k-clusters. This was performed for each phase-based coordination pattern obtained using the k-means algorithm and was denoted structure-function correlation (SFC). We then reorganized the patterns' labels, their unique associated integer between 1 and k, such that the new 'first' pattern would be the pattern with the lowest SFC, and the 'k^{th}' pattern the one with the highest correlation to the anatomy (i.e. structure). Last, we computed the linear slope coefficient of the relationship between the occurrence rate of each centroid and the corresponding centroid/anatomical correlation (i.e. the SFC) to establish a possible tendency for functional states with higher (or lower) correlation to the anatomy.

Brain States' Presence Rate Distribution and Shannon Entropy

For each condition, we computed the histogram associated with the total time of visits of each pattern. This histogram, after normalization, corresponds to the probability distribution of the patterns' occurrence. For each of the normalized histogram of occurrence, and each value of k in the k-means algorithm, we obtained the Shannon entropy (Shannon, 1948) as follows:

$$S = -\sum_i P_i \log_2 P_i$$

Where P_i is the probability (normalized histogram) of visit for each pattern in each brain state (condition).

Markov Chain

For every TR, the k-means algorithm assigns the index of the closest centroid to the corresponding empirical phase coherence matrix, resulting in a sequence of indexes (integers, between 1 and k). We reckon the sequence of "patterns visited" as a sequence of random variables that jumps from one pattern to another pattern with a certain probability given by the empirical frequencies in which these transitioning events happen in the sequence. From these empirical frequencies, we built a Markov Chain, as done previously (Demertzi et al., 2019). More specifically, we counted the number of transitions between all pairs of patterns without considering self-transitions (which correspond to remaining in the same pattern) and normalized these counts to obtain a Markov transition probability matrix $\mathbf{P}$.

Statistical Analysis

To assess the statistical significance of comparing different conditions and differences in occurrence rates, slopes' coefficient, and Shannon entropy, we performed independent t-test with Bonferonni correction between the awake and anesthesia conditions before any stimulation and all their associated stimulation conditions and reported the associated *p* values. We also performed three or two-way ANOVA to confirm that the obtained results of comparing two conditions together (with corrections for multiple comparisons) are consistent with comparing the conditions given the independent variables at play: during/after stimulation, amperage/montage used, and the animal ; and to evaluate possible interactions between said variables.

All these analyses are shown in table form (Table 4) following APA standards by reporting the means and standard deviations, the statistics (T-values or F-values), the degrees of freedom and the *p* values, all to two significant digits. For the ANOVA tests, we also report the sum of squares.

To ensure the reliability of the transition probabilities, we performed a bootstrap method that breaks the temporal dependencies in the chain of visited states. We randomized the order of brain states' appearance, thus conserving the overall statistics but breaking the temporal dependence between specific pairs of visited states. We performed this randomization 10.000 times per condition and computed as many transition matrices. We asserted that certain states' transitions truly reflected a stochastic process and were hence not due to chance by verifying if the empirical transition matrices were above the confidence interval defined by successively stricter confidence levels: 90%, 95%, and 99%. This also allows us to somewhat compensate for the animal-specific effects by discarding them. Finally, for the transitions that did pass at least the 90% confidence interval test, we compared, using independent t-tests with Bonferonni correction, the transition probabilities between conditions and reported the associated *p* values.

All these analyses were performed using customized codes available on an open Github repository for transparency, reproducibility, and open-science (https://github.com/Krigsa/phase_coherence_kmeans). Known Python libraries such as *add_state_annot* (Charlier et al., 2022) or *Scipy* (Virtanen et al., 2020) were used to perform the statistical analysis notably.

ACKNOWLEDGEMENTS.

The research was supported by the Institut National de la Santé et de la Recherche Médicale (to G.H. and B.J.), the Fondation pour la Recherche Médicale (FRM grant number ECO20160736100, to J.T.), FNRS Belgium (project MIS/VA - F.4523.21, to C.M.S.), grant Embodied-Time (40011405, to C.M.S.), Centre National de la Recherche Scientifique and the European Community (Human Brain Project, H2020-945538, to A.D. and R.C.), the Fondation Bettencourt Schueller (to B.J.), Fondation de France (to B.J.), Human Brain Project (Corticity project FLAC-ERA JTC2017, to B.J.), UVSQ (to B.J.), Commissariat à l'Energie Atomique (to B.J.), Collège de France (to B.J.).

References

Alfonsi V, D'Atri A, Scarpelli S, Gorgoni M, Giacinti F, Annarumma L, Salfi F, Amicucci G, Corigliano D, De Gennaro L. 2023. The effects of bifrontal anodal transcranial direct current stimulation (tDCS) on sleepiness and vigilance in partially sleep-deprived subjects: A multidimensional study. *J Sleep Res* **32**:e13869.

Allen EA, Damaraju E, Plis SM, Erhardt EB, Eichele T, Calhoun VD. 2014. Tracking whole-brain connectivity dynamics in the resting state. *Cereb Cortex* **24**:663–676.

Alonso Martínez S, Deco G, Ter Horst GJ, Cabral J. 2020. The Dynamics of Functional Brain Networks Associated With Depressive Symptoms in a Nonclinical Sample. *Front Neural Circuits* **14**:570583.

Angelakis E, Liouta E, Andreadis N, Korfias S, Ktonas P, Stranjalis G, Sakas DE. 2014. Transcranial direct current stimulation effects in disorders of consciousness. *Arch Phys Med Rehabil* **95**:283–289.

Annarumma L, D'Atri A, Alfonsi V, De Gennaro L. 2018. The Efficacy of Transcranial Current Stimulation Techniques to Modulate Resting-State EEG, to Affect Vigilance and to Promote Sleepiness. *Brain Sci* **8**. doi:10.3390/brainsci8070137

Antal A, Terney D, Poreisz C, Paulus W. 2007. Towards unravelling task-related modulations of neuroplastic changes induced in the human motor cortex. *Eur J Neurosci* **26**:2687–2691.

Axelrod V, Rees G, Lavidor M, Bar M. 2015. Increasing propensity to mind-wander with transcranial direct current stimulation. *Proc Natl Acad Sci U S A* **112**:3314–3319.

Baker AP, Brookes MJ, Rezek IA, Smith SM, Behrens T, Probert Smith PJ, Woolrich M. 2014. Fast transient networks in spontaneous human brain activity. *Elife* **3**:e01867.

Bakker R, Wachtler T, Diesmann M. 2012. CoCoMac 2.0 and the future of tract-tracing databases. *Front Neuroinform* **6**:30.

Barttfeld P, Uhrig L, Sitt JD, Sigman M, Jarraya B, Dehaene S. 2015. Signature of consciousness in the dynamics of resting-state brain activity. *Proc Natl Acad Sci U S A* **112**:887–892.

Bekinschtein TA, Dehaene S, Rohaut B, Tadel F, Cohen L, Naccache L. 2009. Neural signature of the conscious processing of auditory regularities. *Proc Natl Acad Sci U S A* **106**:1672–1677.

Bikson M, Inoue M, Akiyama H, Deans JK, Fox JE, Miyakawa H, Jefferys JGR. 2004. Effects of uniform extracellular DC electric fields on excitability in rat hippocampal slices in vitro. *J Physiol* **557**:175–190.

Bikson M, Name A, Rahman A. 2013. Origins of specificity during tDCS: anatomical, activity-selective, and input-bias mechanisms. *Front Hum Neurosci* **7**:688.

Boly M, Phillips C, Tshibanda L, Vanhaudenhuyse A, Schabus M, Dang-Vu TT, Moonen G, Hustinx R, Maquet P, Laureys S. 2008. Intrinsic brain activity in altered states of consciousness: how conscious is the default mode of brain function? *Ann N Y Acad Sci* **1129**:119–129.

Bracewell RN. 2000. The Fourier Transform and Its Applications. McGraw Hill.

Cabral J, Vidaurre D, Marques P, Magalhães R, Silva Moreira P, Miguel Soares J, Deco G, Sousa N, Kringelbach ML. 2017. Cognitive performance in healthy older adults relates to spontaneous switching between states of functional connectivity during rest. *Sci Rep* **7**:5135.

Calhoun VD, Miller R, Pearlson G, Adalı T. 2014. The chronnectome: time-varying connectivity networks as the next frontier in fMRI data discovery. *Neuron* **84**:262–274.

Castro P, Luppi A, Tagliazucchi E, S-Perl Y, Naci L, Owen AM, Sitt JD, Destexhe A, Cofré R. 2023. Dynamical structure-function correlations provide robust and generalizable signatures of consciousness in humans. *bioRxiv*. doi:10.1101/2023.12.19.572402

Charlier F, Weber M, Izak D, Harkin E, Magnus M, Lalli J, Fresnais L, Chan M, Markov N, Amsalem O, Proost S, Krasoulis A, getzze, Repplinger S. 2022. trevismd/statannotations: v0.5. Zenodo. doi:10.5281/ZENODO.7213391

Conscious Processing and the Global Neuronal Workspace Hypothesis. 2020. . *Neuron* **105**:776–798.

Coulborn S, Fernández-Espejo D. 2022. Prefrontal tDCS is unable to modulate mind wandering propensity or underlying functional or effective brain connectivity. *Sci Rep* **12**:18021.

Dai J, Wang H, Yang L, Wang C, Cheng S, Zhang T, Ma J, Wen Z, Cao X, Hu W. 2022. The neuroelectrophysiological and behavioral effects of transcranial direct current stimulation on executive vigilance under a continuous monotonous condition. *Front Neurosci* **16**:910457.
Dalong G, Jiyuan L, Ying Z, Lei Z, Yanhong H, Yongcong S. 2020. Transcranial direct current stimulation reconstructs diminished thalamocortical connectivity during prolonged resting wakefulness: a resting-state fMRI pilot study. *Brain Imaging Behav* **14**:278–288.
Damoiseaux JS, Rombouts SARB, Barkhof F, Scheltens P, Stam CJ, Smith SM, Beckmann CF. 2006. Consistent resting-state networks across healthy subjects. *Proc Natl Acad Sci U S A* **103**:13848–13853.
Datta A, Bansal V, Diaz J, Patel J, Reato D, Bikson M. 2009. Gyri-precise head model of transcranial direct current stimulation: improved spatial focality using a ring electrode versus conventional rectangular pad. *Brain Stimul* **2**:201–7, 207.e1.
Deco G, Jirsa VK, McIntosh AR. 2013. Resting brains never rest: computational insights into potential cognitive architectures. *Trends Neurosci* **36**:268–274.
Deco G, Jirsa VK, McIntosh AR. 2011. Emerging concepts for the dynamical organization of resting-state activity in the brain. *Nat Rev Neurosci* **12**:43–56.
Demertzi A, Tagliazucchi E, Dehaene S, Deco G, Barttfeld P, Raimondo F, Martial C, Fernández-Espejo D, Rohaut B, Voss HU, Schiff ND, Owen AM, Laureys S, Naccache L, Sitt JD. 2019. Human consciousness is supported by dynamic complex patterns of brain signal coordination. *Sci Adv* **5**:eaat7603.
Dmochowski JP, Datta A, Bikson M, Su Y, Parra LC. 2011. Optimized multi-electrode stimulation increases focality and intensity at target. *J Neural Eng* **8**:046011.
Ensel S, Uhrig L, Ozkirli A, Hoffner G, Tasserie J, Dehaene S, Van De Ville D, Jarraya B, Pirondini E. 2023. Transient brain activity dynamics discriminate levels of consciousness during anesthesia. *bioRxiv*. doi:10.1101/2023.10.09.560209
Fonteneau C, Mondino M, Arns M, Baeken C, Bikson M, Brunoni AR, Burke MJ, Neuvonen T, Padberg F, Pascual-Leone A, Poulet E, Ruffini G, Santarnecchi E, Sauvaget A, Schellhorn K, Suaud-Chagny M-F, Palm U, Brunelin J. 2019. Sham tDCS: A hidden source of variability? Reflections for further blinded, controlled trials. *Brain Stimul* **12**:668–673.
Fox MD, Corbetta M, Snyder AZ, Vincent JL, Raichle ME. 2006. Spontaneous neuronal activity distinguishes human dorsal and ventral attention systems. *Proc Natl Acad Sci U S A* **103**:10046–10051.
Frase L, Maier JG, Zittel S, Freyer T, Riemann D, Normann C, Feige B, Nitsche MA, Nissen C. 2015. Bifrontal Anodal Transcranial Direct Current Stimulation (tDCS) Improves Daytime Vigilance and Sleepiness in a Patient With Organic Hypersomnia Following Reanimation. *Brain Stimul* **8**:844–846.
Frase L, Piosczyk H, Zittel S, Jahn F, Selhausen P, Krone L, Feige B, Mainberger F, Maier JG, Kuhn M, Klöppel S, Normann C, Sterr A, Spiegelhalder K, Riemann D, Nitsche MA, Nissen C. 2016. Modulation of Total Sleep Time by Transcranial Direct Current Stimulation (tDCS). *Neuropsychopharmacology* **41**:2577–2586.
Frey S, Pandya DN, Chakravarty MM, Bailey L, Petrides M, Collins DL. 2011. An MRI based average macaque monkey stereotaxic atlas and space (MNI monkey space). *Neuroimage* **55**:1435–1442.
Glerean E, Salmi J, Lahnakoski JM, Jääskeläinen IP, Sams M. 2012. Functional magnetic resonance imaging phase synchronization as a measure of dynamic functional connectivity. *Brain Connect* **2**:91–101.
Golkowski D, Larroque SK, Vanhaudenhuyse A, Plenevaux A, Boly M, Di Perri C, Ranft A, Schneider G, Laureys S, Jordan D, Bonhomme V, Ilg R. 2019. Changes in Whole Brain Dynamics and Connectivity Patterns during Sevoflurane- and Propofol-induced Unconsciousness Identified by Functional Magnetic Resonance Imaging. *Anesthesiology* **130**:898–911.
Guidetti M, Arlotti M, Bocci T, Bianchi AM, Parazzini M, Ferrucci R, Priori A. 2022. Electric Fields Induced in the Brain by Transcranial Electric Stimulation: A Review of In Vivo Recordings. *Biomedicines* **10**. doi:10.3390/biomedicines10102333
Gu Z, Chen W, Lu Q, Dai J, Hu S, Xu K, Geng Y, Zhu Y, Xu B, Dai W, Shen Y. 2022. Anodal

high-definition transcranial direct current stimulation reduces heart rate and modulates heart-rate variability in healthy young people: A randomized cross-controlled trial. *Front Cardiovasc Med* **9**:1070157.
Hermann B, Raimondo F, Hirsch L, Huang Y, Denis-Valente M, Pérez P, Engemann D, Faugeras F, Weiss N, Demeret S, Rohaut B, Parra LC, Sitt JD, Naccache L. 2020. Combined behavioral and electrophysiological evidence for a direct cortical effect of prefrontal tDCS on disorders of consciousness. *Sci Rep* **10**:4323.
Hindriks R, Adhikari MH, Murayama Y, Ganzetti M, Mantini D, Logothetis NK, Deco G. 2016. Can sliding-window correlations reveal dynamic functional connectivity in resting-state fMRI? *Neuroimage* **127**:242–256.
Hsu G, Shereen AD, Cohen LG, Parra LC. 2023. Robust enhancement of motor sequence learning with 4 mA transcranial electric stimulation. *Brain Stimul* **16**:56–67.
Huang Y, Su Y, Rorden C, Dmochowski J, Datta A, Parra LC. 2012. An automated method for high-definition transcranial direct current stimulation modeling. *Conf Proc IEEE Eng Med Biol Soc* **2012**:5376–5379.
Huang Z, Zhang J, Wu J, Mashour GA, Hudetz AG. 2020. Temporal circuit of macroscale dynamic brain activity supports human consciousness. *Sci Adv* **6**:eaaz0087.
Karahanoğlu FI, Van De Ville D. 2015. Transient brain activity disentangles fMRI resting-state dynamics in terms of spatially and temporally overlapping networks. *Nat Commun* **6**:7751.
Kato R, Solt K. 2021. Prehabilitation With Brain Stimulation? *Anesth Analg*.
Kötter R, Wanke E. 2005. Mapping brains without coordinates. *Philos Trans R Soc Lond B Biol Sci* **360**:751–766.
Krone L, Frase L, Piosczyk H, Selhausen P, Zittel S, Jahn F, Kuhn M, Feige B, Mainberger F, Klöppel S, Riemann D, Spiegelhalder K, Baglioni C, Sterr A, Nissen C. 2017. Top-down control of arousal and sleep: Fundamentals and clinical implications. *Sleep Med Rev* **31**:17–24.
Lefaucheur J-P, Antal A, Ayache SS, Benninger DH, Brunelin J, Cogiamanian F, Cotelli M, De Ridder D, Ferrucci R, Langguth B, Marangolo P, Mylius V, Nitsche MA, Padberg F, Palm U, Poulet E, Priori A, Rossi S, Schecklmann M, Vanneste S, Ziemann U, Garcia-Larrea L, Paulus W. 2017. Evidence-based guidelines on the therapeutic use of transcranial direct current stimulation (tDCS). *Clin Neurophysiol* **128**:56–92.
Lefaucheur J-P, Wendling F. 2019. Mechanisms of action of tDCS: A brief and practical overview. *Neurophysiol Clin* **49**:269–275.
Li LM, Violante IR, Leech R, Ross E, Hampshire A, Opitz A, Rothwell JC, Carmichael DW, Sharp DJ. 2019. Brain state and polarity dependent modulation of brain networks by transcranial direct current stimulation. *Hum Brain Mapp* **40**:904–915.
Liu Z, Zhang X, Yu B, Wang J, Lu X. 2023. Effectiveness on level of consciousness of non-invasive neuromodulation therapy in patients with disorders of consciousness: a systematic review and meta-analysis. *Front Hum Neurosci* **17**:1129254.
Louviot S, Tyvaert L, Maillard LG, Colnat-Coulbois S, Dmochowski J, Koessler L. 2022. Transcranial Electrical Stimulation generates electric fields in deep human brain structures. *Brain Stimul* **15**:1–12.
Luppi AI, Golkowski D, Ranft A, Ilg R, Jordan D, Menon DK, Stamatakis EA. 2021. Brain network integration dynamics are associated with loss and recovery of consciousness induced by sevoflurane. *Hum Brain Mapp* **42**:2802–2822.
Luppi AI, Uhrig L, Tasserie J, Signorelli CM, Stamatakis EA, Destexhe A, Jarraya B, Cofre R. 2024. Local orchestration of distributed functional patterns supporting loss and restoration of consciousness in the primate brain. *Nat Commun* **15**:2171.
Maeoka H, Matsuo A, Hiyamizu M, Morioka S, Ando H. 2012. Influence of transcranial direct current stimulation of the dorsolateral prefrontal cortex on pain related emotions: a study using electroencephalographic power spectrum analysis. *Neurosci Lett* **512**:12–16.
Mansouri MT, García PS. 2021. Repetitive Anodal Transcranial Direct Current Stimulation Hastens Isoflurane-Induced Emergence and Recovery and Enhances Memory in Healthy Rats. *Anesth Analg* **132**:1347–1358.
McCormick DA. 1992. Neurotransmitter actions in the thalamus and cerebral cortex and their role

in neuromodulation of thalamocortical activity. *Prog Neurobiol* **39**:337–388.
McIntire LK, McKinley RA, Goodyear C, Nelson J. 2014. A comparison of the effects of transcranial direct current stimulation and caffeine on vigilance and cognitive performance during extended wakefulness. *Brain Stimul* **7**:499–507.
Mortaheb S, Van Calster L, Raimondo F, Klados MA, Boulakis PA, Georgoula K, Majerus S, Van De Ville D, Demertzi A. 2022. Mind blanking is a distinct mental state linked to a recurrent brain profile of globally positive connectivity during ongoing mentation. *Proc Natl Acad Sci U S A* **119**:e2200511119.
Narmashiri A, Akbari F. 2023. The Effects of Transcranial Direct Current Stimulation (tDCS) on the Cognitive Functions: A Systematic Review and Meta-analysis. *Neuropsychol Rev*. doi:10.1007/s11065-023-09627-x
Nawani H, Mittner M, Csifcsák G. 2023. Modulation of mind wandering using transcranial direct current stimulation: A meta-analysis based on electric field modeling. *Neuroimage* **272**:120051.
Nitsche MA, Bikson M. 2017. Extending the parameter range for tDCS: Safety and tolerability of 4 mA stimulation. *Brain Stimul*.
Nitsche MA, Paulus W. 2000. Excitability changes induced in the human motor cortex by weak transcranial direct current stimulation. *J Physiol* **527 Pt 3**:633–639.
Patel SR, Ballesteros JJ, Ahmed OJ, Huang P, Briscoe J, Eskandar EN, Ishizawa Y. 2020. Dynamics of recovery from anaesthesia-induced unconsciousness across primate neocortex. *Brain* **143**:833–843.
Peng Y, Zhao J, Lu X, Dong J, Zhang S, Zhang J, Liu H, Zheng X, Wang X, Lan Y, Yan T. 2022. Efficacy of Transcranial Direct Current Stimulation Over Dorsolateral Prefrontal Cortex in Patients With Minimally Conscious State. *Front Neurol* **13**:821286.
Perri RL, Di Filippo G. 2023. Alteration of hypnotic experience following transcranial electrical stimulation of the left prefrontal cortex. *Int J Clin Health Psychol* **23**:100346.
Perri RL, Perrotta D, Rossani F, Pekala RJ. 2022. Boosting the hypnotic experience. Inhibition of the dorsolateral prefrontal cortex alters hypnotizability and sense of agency. A randomized, double-blind and sham-controlled tDCS study. *Behav Brain Res* **425**:113833.
Polanía R, Paulus W, Nitsche MA. 2012. Modulating cortico-striatal and thalamo-cortical functional connectivity with transcranial direct current stimulation. *Hum Brain Mapp* **33**:2499–2508.
Preti MG, Bolton TA, Van De Ville D. 2017. The dynamic functional connectome: State-of-the-art and perspectives. *Neuroimage* **160**:41–54.
Raichle ME, MacLeod AM, Snyder AZ, Powers WJ, Gusnard DA, Shulman GL. 2001. A default mode of brain function. *Proc Natl Acad Sci U S A* **98**:676–682.
Rebollo B, Telenczuk B, Navarro-Guzman A, Destexhe A, Sanchez-Vives MV. 2021. Modulation of intercolumnar synchronization by endogenous electric fields in cerebral cortex. *Sci Adv* **7**. doi:10.1126/sciadv.abc7772
Rodrigues B, Barboza CA, Moura EG, Ministro G, Ferreira-Melo SE, Castaño JB, Nunes WMS, Mostarda C, Coca A, Vianna LC, Moreno-Junior H. 2022. Acute and Short-Term Autonomic and Hemodynamic Responses to Transcranial Direct Current Stimulation in Patients With Resistant Hypertension. *Front Cardiovasc Med* **9**:853427.
Saturnino GB, Puonti O, Nielsen JD, Antonenko D, Madsen KH, Thielscher A. 2019. SimNIBS 2.1: A Comprehensive Pipeline for Individualized Electric Field Modelling for Transcranial Brain Stimulation In: Makarov S, Horner M, Noetscher G, editors. Brain and Human Body Modeling: Computational Human Modeling at EMBC 2018. Cham (CH): Springer.
Shannon CE. 1948. A mathematical theory of communication.
Shen K, Bezgin G, Schirner M, Ritter P, Everling S, McIntosh AR. 2019. A macaque connectome for large-scale network simulations in TheVirtualBrain. *Sci Data* **6**:123.
Signorelli CM, Uhrig L, Kringelbach M, Jarraya B, Deco G. 2021. Hierarchical disruption in the cortex of anesthetized monkeys as a new signature of consciousness loss. *Neuroimage* **227**:117618.
Steriade MM, McCarley RW. 2013. Brainstem Control of Wakefulness and Sleep. Springer Science & Business Media.

Tagliazucchi E, Laufs H. 2014. Decoding wakefulness levels from typical fMRI resting-state data reveals reliable drifts between wakefulness and sleep. *Neuron* **82**:695–708.
Tasserie J, Uhrig L, Sitt JD, Manasova D, Dupont M, Dehaene S, Jarraya B. 2022. Deep brain stimulation of the thalamus restores signatures of consciousness in a nonhuman primate model. *Sci Adv* **8**:eabl5547.
Thibaut A, Bruno M-A, Ledoux D, Demertzi A, Laureys S. 2014. tDCS in patients with disorders of consciousness: sham-controlled randomized double-blind study. *Neurology* **82**:1112–1118.
Uhrig L, Dehaene S, Jarraya B. 2014. A hierarchy of responses to auditory regularities in the macaque brain. *J Neurosci* **34**:1127–1132.
Uhrig L, Janssen D, Dehaene S, Jarraya B. 2016. Cerebral responses to local and global auditory novelty under general anesthesia. *Neuroimage* **141**:326–340.
Uhrig L, Sitt JD, Jacob A, Tasserie J, Barttfeld P, Dupont M, Dehaene S, Jarraya B. 2018. Resting-state Dynamics as a Cortical Signature of Anesthesia in Monkeys. *Anesthesiology* **129**:942–958.
Vanduffel W, Fize D, Mandeville JB, Nelissen K, Van Hecke P, Rosen BR, Tootell RB, Orban GA. 2001. Visual motion processing investigated using contrast agent-enhanced fMRI in awake behaving monkeys. *Neuron* **32**:565–577.
Vincent JL, Snyder AZ, Fox MD, Shannon BJ, Andrews JR, Raichle ME, Buckner RL. 2006. Coherent spontaneous activity identifies a hippocampal-parietal memory network. *J Neurophysiol* **96**:3517–3531.
Virtanen P, Gommers R, Oliphant TE, Haberland M, Reddy T, Cournapeau D, Burovski E, Peterson P, Weckesser W, Bright J, van der Walt SJ, Brett M, Wilson J, Millman KJ, Mayorov N, Nelson ARJ, Jones E, Kern R, Larson E, Carey CJ, Polat İ, Feng Y, Moore EW, VanderPlas J, Laxalde D, Perktold J, Cimrman R, Henriksen I, Quintero EA, Harris CR, Archibald AM, Ribeiro AH, Pedregosa F, van Mulbregt P, SciPy 1.0 Contributors. 2020. SciPy 1.0: fundamental algorithms for scientific computing in Python. *Nat Methods* **17**:261–272.
Vohryzek J, Deco G, Cessac B, Kringelbach ML, Cabral J. 2020. Ghost Attractors in Spontaneous Brain Activity: Recurrent Excursions Into Functionally-Relevant BOLD Phase-Locking States. *Front Syst Neurosci* **14**:20.
Wirth M, Rahman RA, Kuenecke J, Koenig T, Horn H, Sommer W, Dierks T. 2011. Effects of transcranial direct current stimulation (tDCS) on behaviour and electrophysiology of language production. *Neuropsychologia* **49**:3989–3998.
Xie H, Gonzalez-Castillo J, Handwerker DA, Bandettini PA, Calhoun VD, Chen G, Damaraju E, Liu X, Mitra S. 2019. Time-varying whole-brain functional network connectivity coupled to task engagement. *Netw Neurosci* **3**:49–66.

Figures

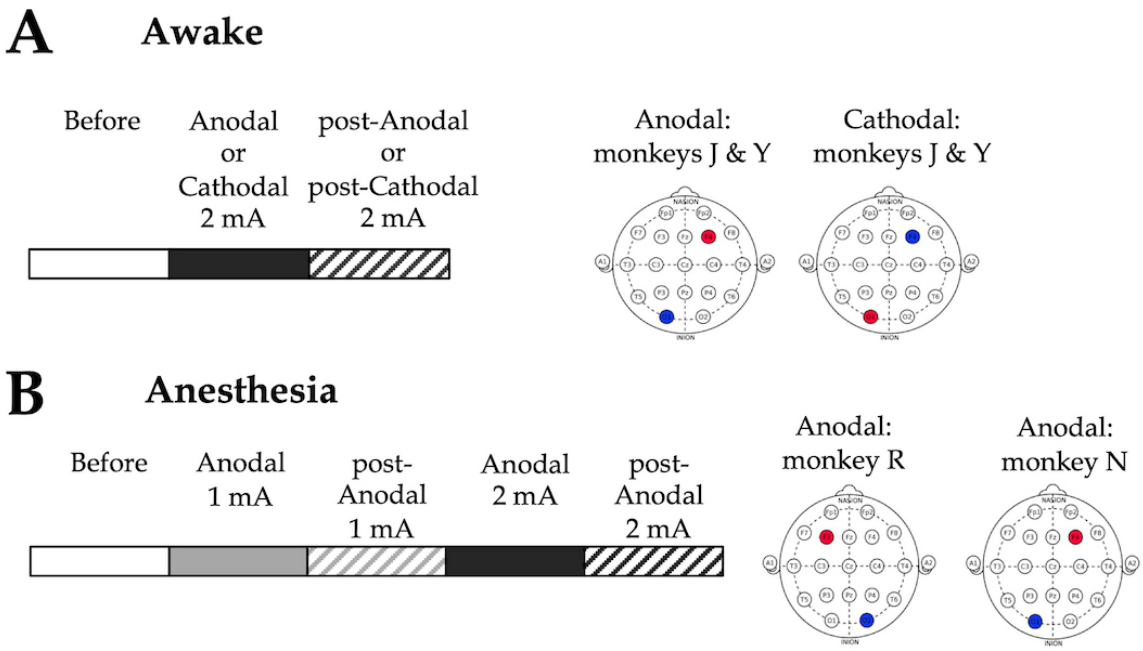

Figure 1. Schematic representation of the experimental designs and HD-tDCS electrode montages employed in the study. A) Awake experiments. fMRI data were acquired before, during, and after 20 min of tDCS stimulation at 2 mA intensity. The anodal electrode (red) was either placed over the right prefrontal cortex (F4) and the cathodal electrode (blue) over the left occipital cortex (O1) ("anodal" montage), or a "reversed" montage was used, with the cathodal electrode over F4 and the anodal electrode over O1 ("cathodal" montage). B) Anesthesia experiments. fMRI data were recorded before, during, and after 20 min of consecutive 1 mA and 2 mA tDCS stimulation. An anodal electrode montage was employed, targeting the left or right prefrontal cortex (F4/O1 or F3/O2) depending on the animal and its anatomical constraints. Before: before stimulation. Anodal and post-Anodal: during and after anodal HD-tDCS of the PFC. Cathodal and post-Cathodal: during and after cathodal HD-tDCS of the PFC.

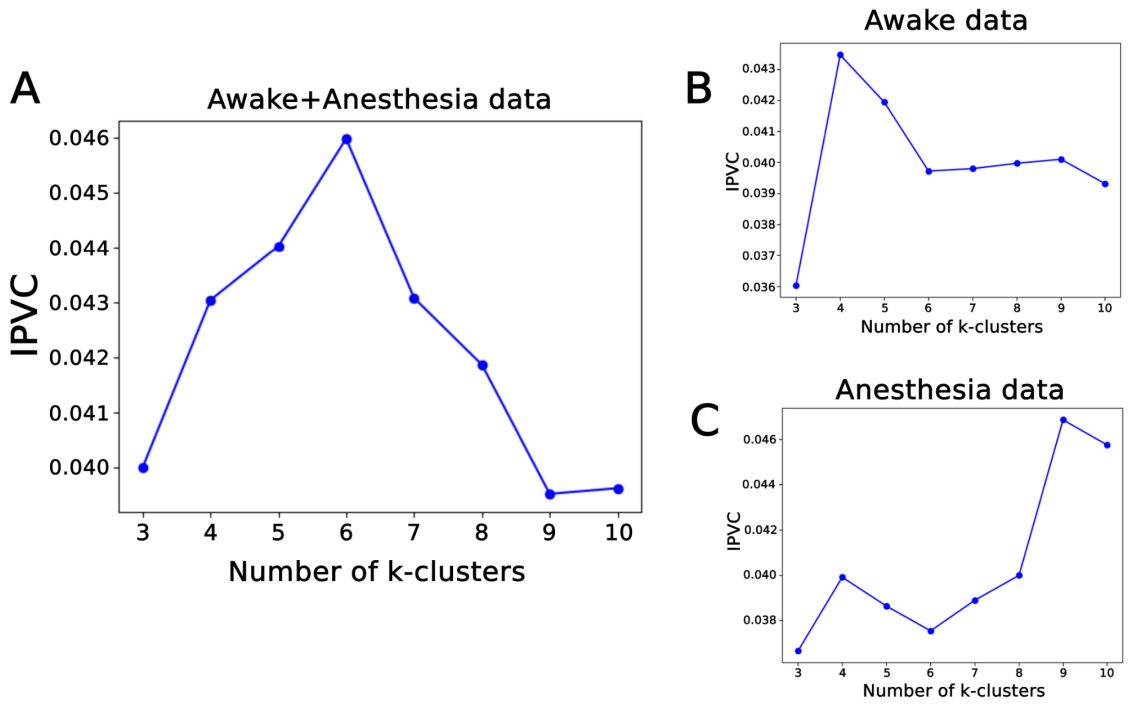

Figure 2. Inter-pattern correlation variance (IPCV), a measure used to identify the optimal number of *k*-clusters (or brain patterns). A) IPCV obtained when awake and anesthesia datasets are considered together. B) IPCV obtained when only the awake dataset is considered. C) IPCV obtained with only the anesthesia dataset.

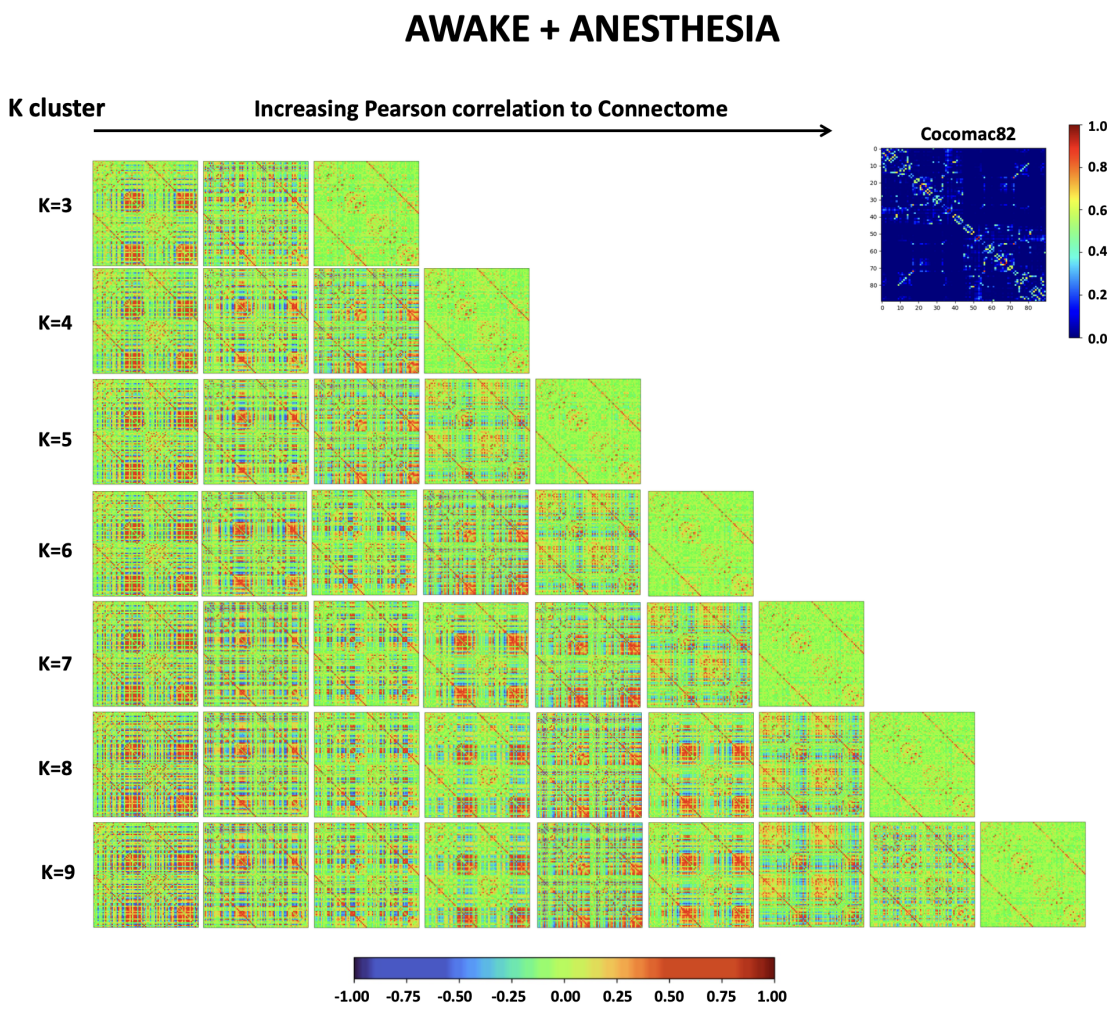

Figure 2 - figure supplement 1. Dynamical functional patterns from awake and anesthesia datasets. Matrix representation of the brain patterns for *k*=3 to 9 number of clusters in the k-means algorithm. The brain patterns were obtained by including all the awake (5 conditions) and anesthesia (5 conditions) data in the analysis and ordered from least (left) to most (right) similarity to the structural connectivity matrix.

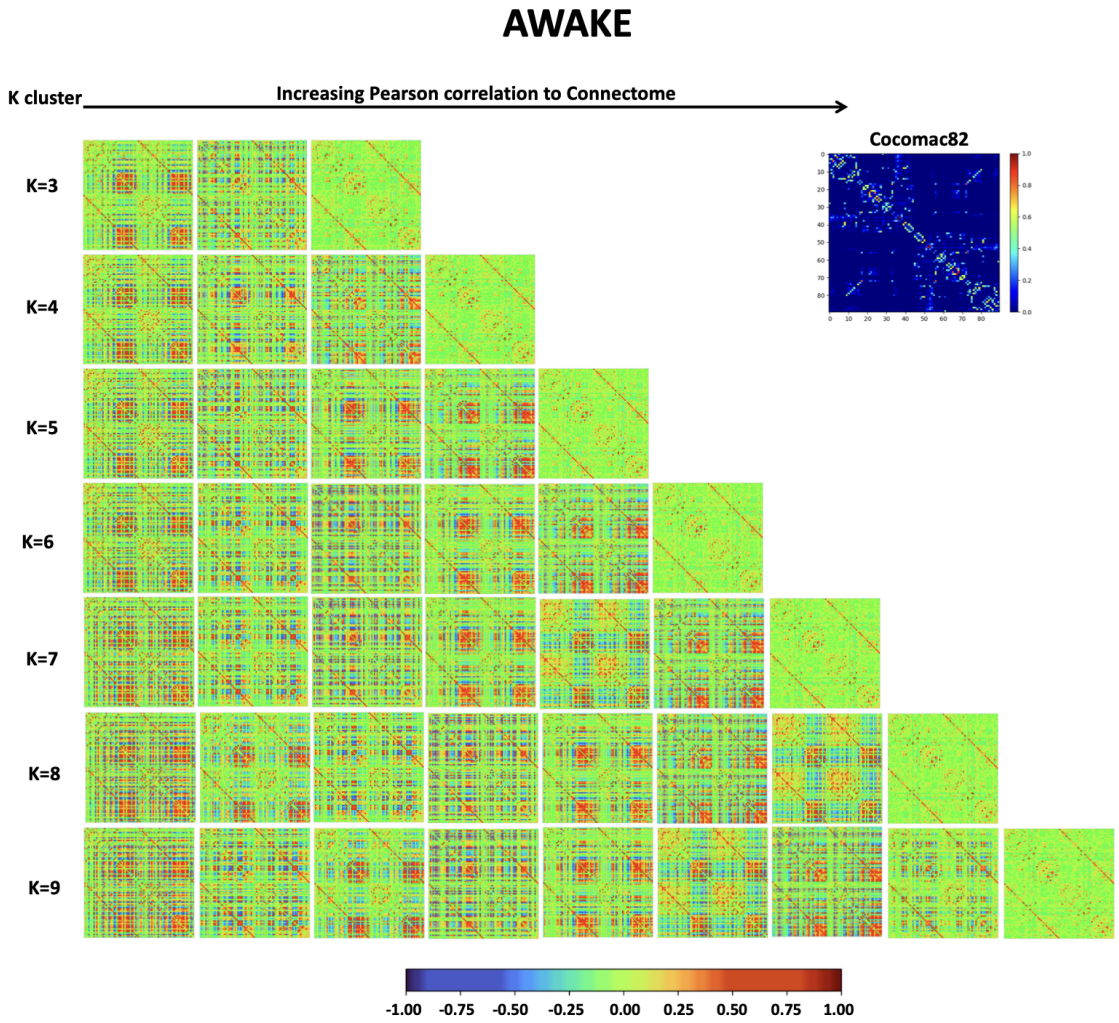

Figure 2 - figure supplement 2. Dynamical functional patterns from the awake dataset. Matrix representation of the brain patterns for *k*=3 to 9 number of clusters in the k-means algorithm. The brain patterns were obtained by including all five awake conditions and were ordered from least (left) to most (right) similarity to the structural connectivity matrix.

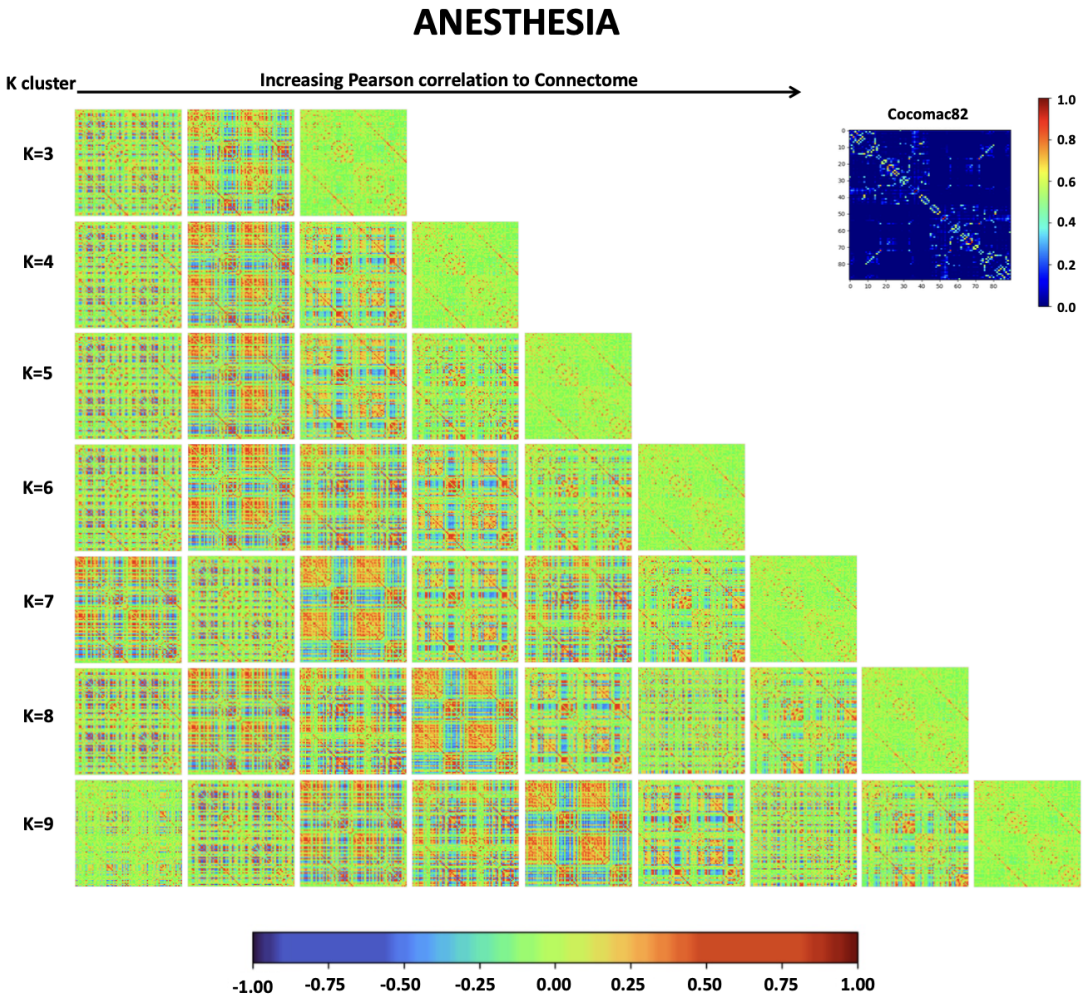

Figure 2 - figure supplement 3. Dynamical functional patterns from the anesthesia dataset. Matrix representation of the brain patterns for *k*=3 to 9 number of clusters in the k-means algorithm. The brain patterns were obtained by including all five anesthesia conditions and were ordered from least (left) to most (right) similarity to the structural connectivity matrix.

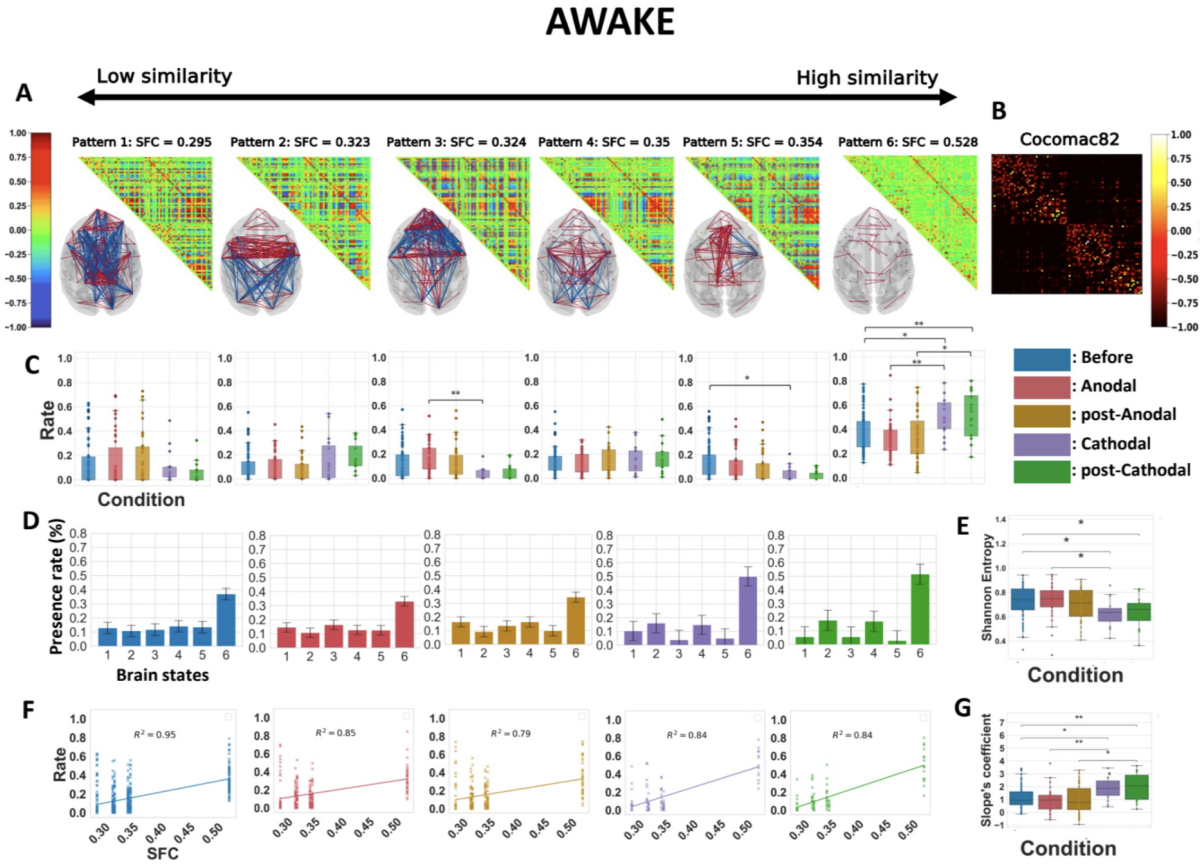

Figure 3. Cathodal but not anodal HD-tDCS of the prefrontal cortex alters the repertoire of functional brain patterns, increases structure-function coupling and decreases Shannon Entropy in awake animals. A) Matrix representation of the brain patterns for *k* = 6, obtained by including all the five awake conditions. Brain coordination patterns are ranked from least (left) to highest (right) correlation to the structural connectivity matrix. Networks are plotted in anatomical space (transverse view), showing only values <-0.5 and >0.5. Red lines represent positive synchronizations between regions of interest, and blue lines represent negative ones. B) Macaque connectome in the CoCoMac82 parcellation. C) Rate of occurrence of each brain connectivity pattern across the five conditions. Boxplots show median occurrence rates with interquartile range and maximum-minimum values (whiskers). D) Barplots of the 6 brain states and their average presence rate over the different conditions. E) Normalized Shannon Entropy as a function of the conditions. F) Rates of occurrence of brain patterns as a function of their similarity in functional and structural connectivity (SFC) for the five conditions. Lines are calculated, per conditions, based on the best linear fit between the average presence rate of each pattern and their SFC. R^2, Spearman correlation. Crosses represent individuals' presence rates. G) Coefficient of the linearly regressed slope across conditions. Before: pre-stimulation, Anodal and post-Anodal: during and after anodal HD-tDCS of the PFC (F4/O1 montage). Cathodal and post-Cathodal: during and after cathodal HD-tDCS of the PFC (O1/F4 montage).

AWAKE

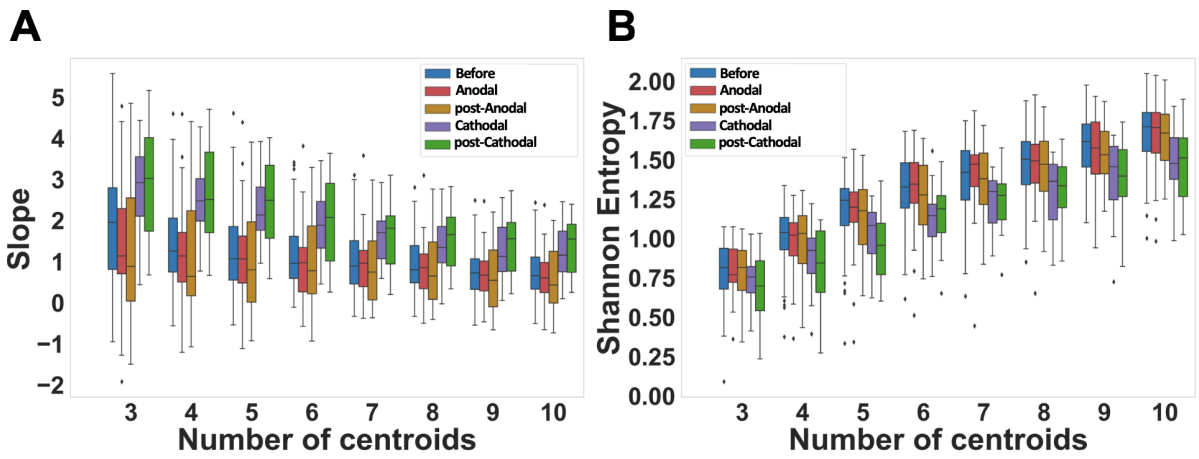

Figure 3 - figure supplement 1. Slope and Shannon Entropy in the awake conditions. Slopes of the linear regression (A) and Shannon Entropy (B) of the distribution of brain patterns occurrences computed for a number of clusters from 3 to 10 in the k-means algorithm. All five awake conditions were included in the analyses. The same relative differences were found for all values of *k* analyzed. In the cathodal prefrontal stimulation conditions, the slopes of the linear regression show a tendency towards anatomically driven dynamics, and the Shannon entropy is lower than in the pre-stimulation and anodal prefrontal stimulation conditions.

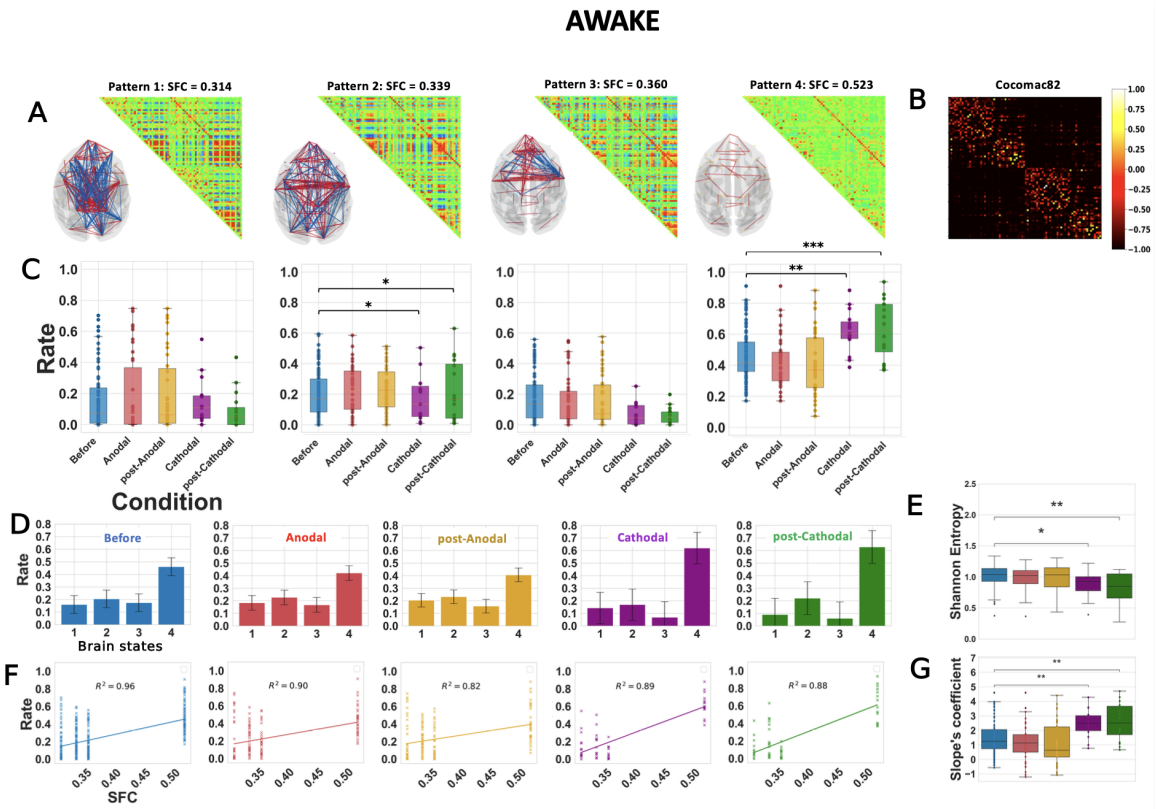

Figure 3 - figure supplement 2. Dynamical functional connectivity analysis of the awake dataset with *k* = 4 numbers of clusters. Similar analysis than in Figure 2 for *k*=4 considering all the five awake conditions. Before: before HD-tDCS in the awake state. Anodal and post-Anodal: during and after anodal HD-tDCS of the PFC (F4/O1 electrode montage) at an intensity of 2 mA. Cathodal and post-Cathodal: during and after cathodal HD-tDCS of the PFC (O1/F4 montage) at an intensity of 2 mA.

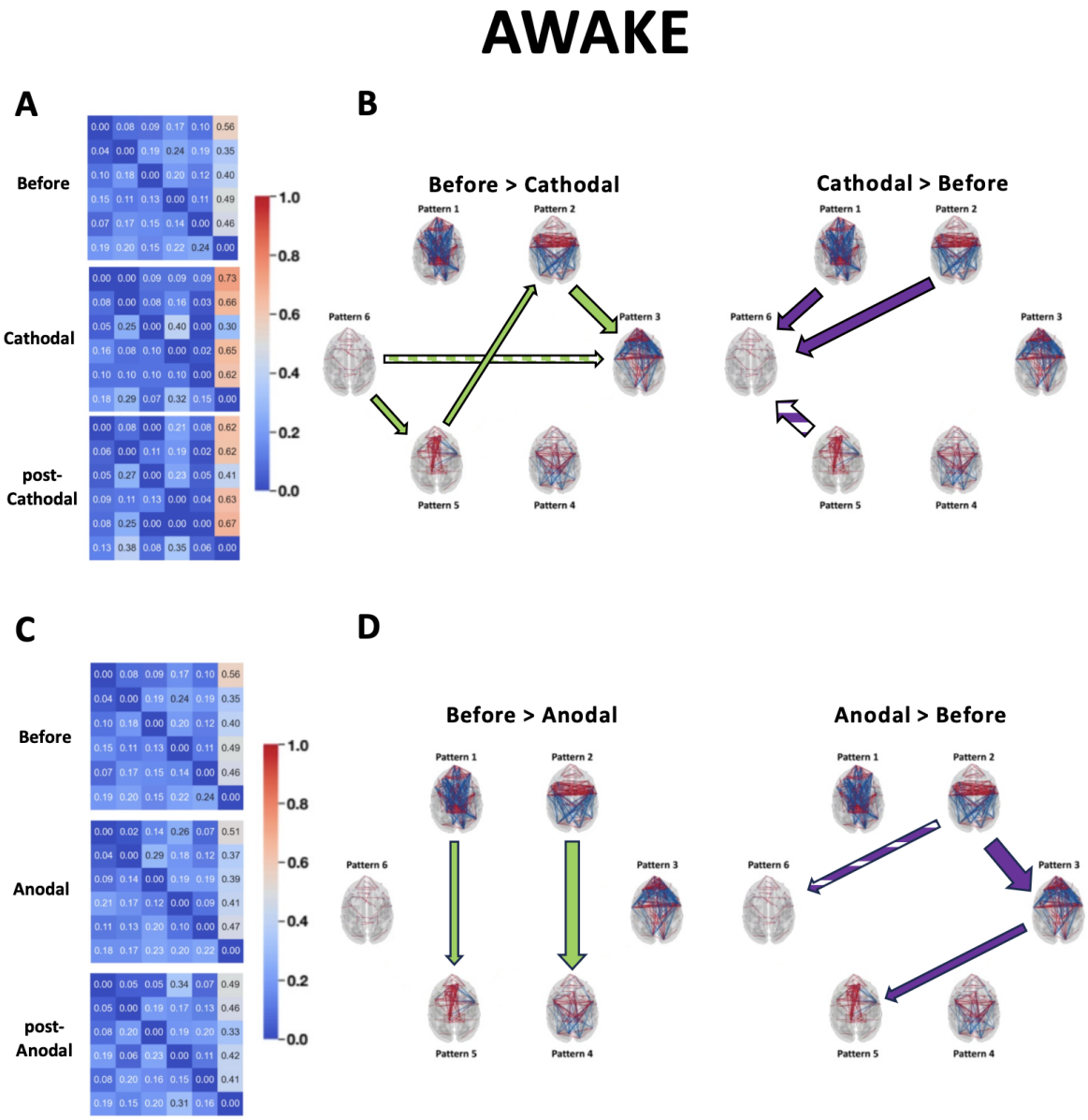

Figure 4. Transition probabilities and Markov chain analysis of the identified brain states during and after cathodal or anodal PFC stimulation in the awake state. A & C) Overall transition probabilities matrices pre-stimulation, during and after cathodal stimulation (A) or during and after anodal stimulation (C). B & D) Left panels: transition probabilities greater before stimulation than during stimulation (full green arrows) or post-stimulation (hashed green arrows). Right panels: transition probabilities greater during (full purple arrows) or after (hashed purple arrows) the stimulation than before. Arrow size indicates *p* value significance. Before: pre-

stimulation. Cathodal and post-Cathodal: during and after cathodal HD-tDCS of the PFC (O1/F4 montage). Anodal and post-Anodal: during and after anodal HD-tDCS of the PFC (F4/O1 montage).

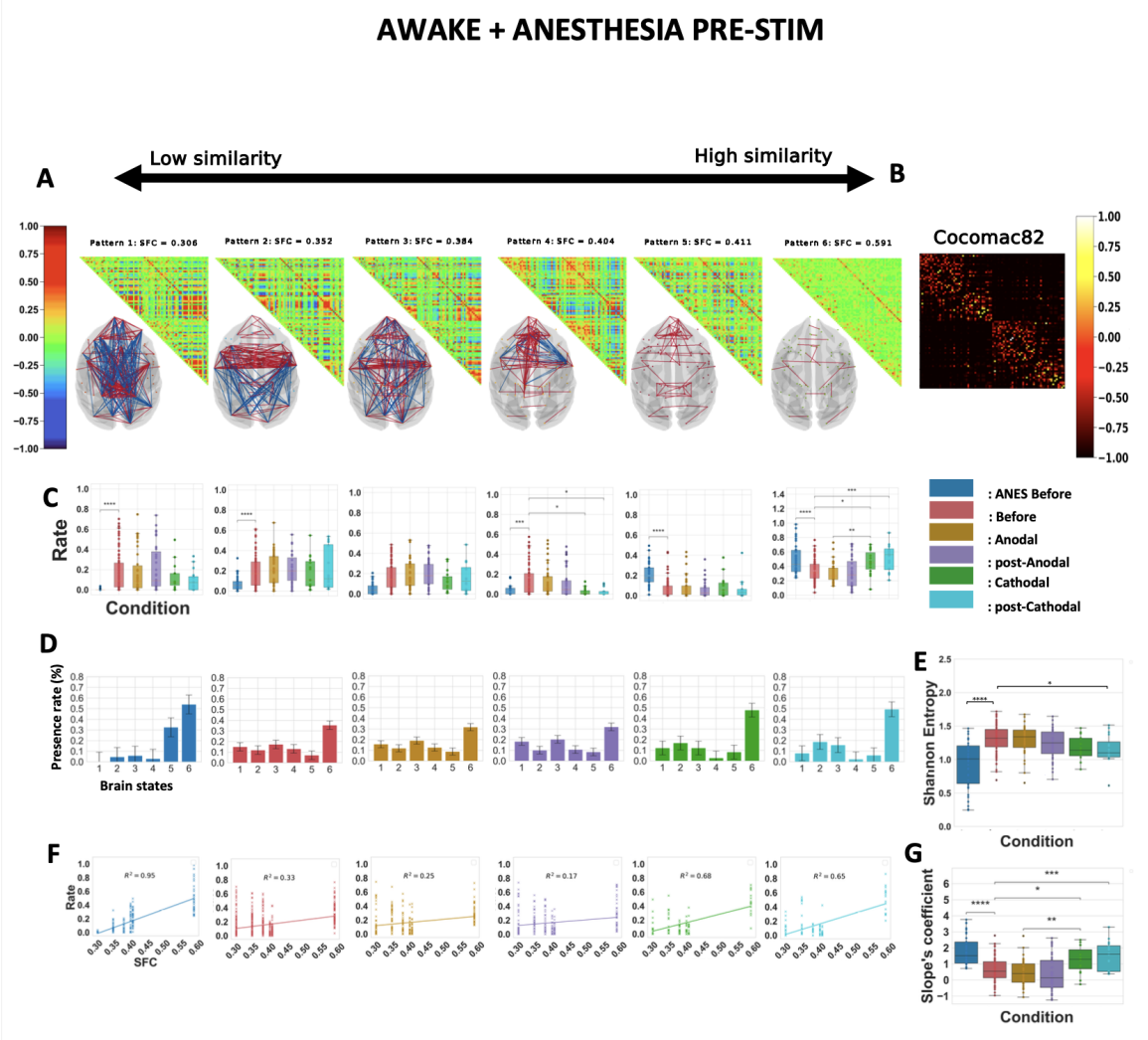

Figure 5. The polarity-dependent effects of prefrontal HD-tDCS on awake brain dynamics resist contrasting with anesthetized dynamics. Similar analysis than in Figure 3 for *k*=6 considering all the five awake conditions plus the anesthesia pre-stimulation condition. ANES Before: before stimulation under anesthesia. Before: before stimulation in the awake state. Anodal and post-Anodal: during and after anodal HD-tDCS of the PFC (F4/O1 montage) in the awake state. Cathodal and post-Cathodal: during and after cathodal HD-tDCS of the PFC (O1/F4 montage) in the awake state.

AWAKE + ANESTHESIA PRE-STIM

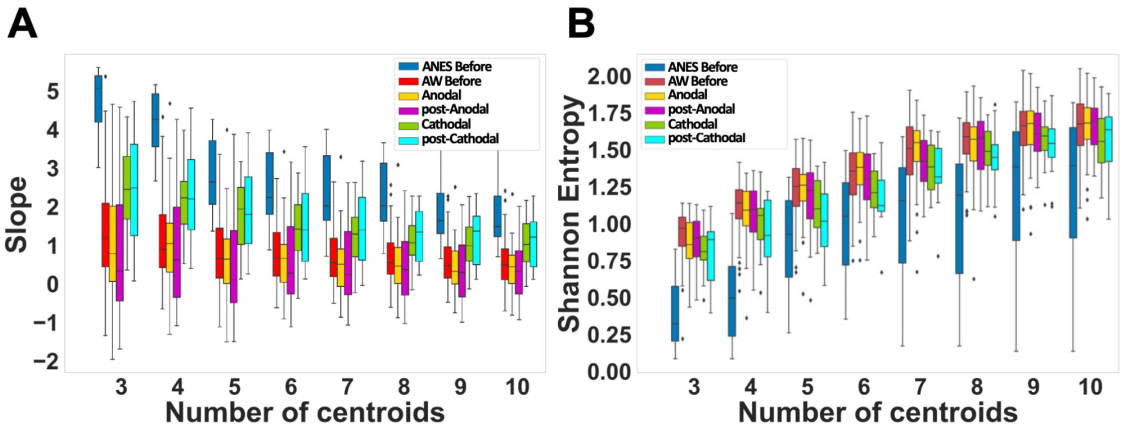

Figure 5 - figure supplement 1. Slope and Shannon Entropy in awake conditions contrasted with anesthesia pre-stimulation condition. Slopes of the linear regression (A) and Shannon Entropy (B) of the distribution of brain patterns occurrences computed for a number of clusters from 3 to 10 in the k-means algorithm. All five awake conditions plus the anesthesia pre-stimulation condition were included in the analyses. The same relative differences were found for all values of *k* analyzed. In the cathodal prefrontal stimulation conditions, the slopes of the linear regression are increased and tend to approach the values of the anesthesia pre-stimulation condition. Similarly, the Shannon entropy is lower in the cathodal stimulation conditions than in the pre-stimulation and anodal prefrontal stimulation conditions and moves towards the value of the anesthesia pre-stimulation condition.

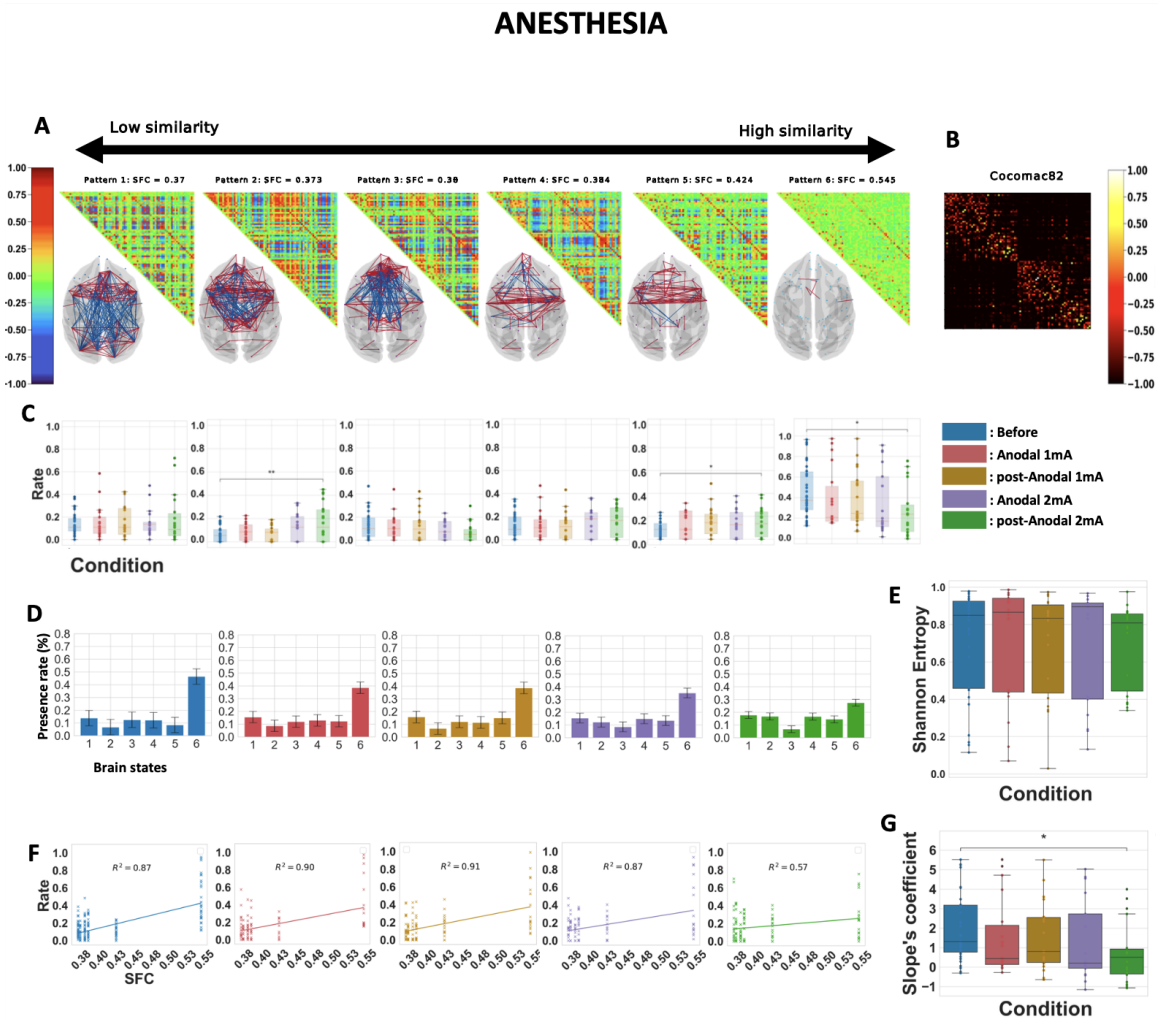

Figure 6. Anodal 2 mA HD-tDCS of the prefrontal cortex modifies cortical brain dynamics and reduces structure-function coupling in anesthetized animals. Similar analysis than in Figures 3 and 5 for *k*=6 considering all the five anesthesia conditions. Before: before stimulation. Anodal 1 mA and post-Anodal 1 mA: during and after anodal HD-tDCS of the PFC (F4/O1 or F3/O2) delivered at an intensity of 1 mA. Anodal 2 mA and post-Anodal 2 mA: during and after anodal HD-tDCS of the PFC (F4/O1 or F3/O2 montage) delivered at an intensity of 2 mA.

ANESTHESIA

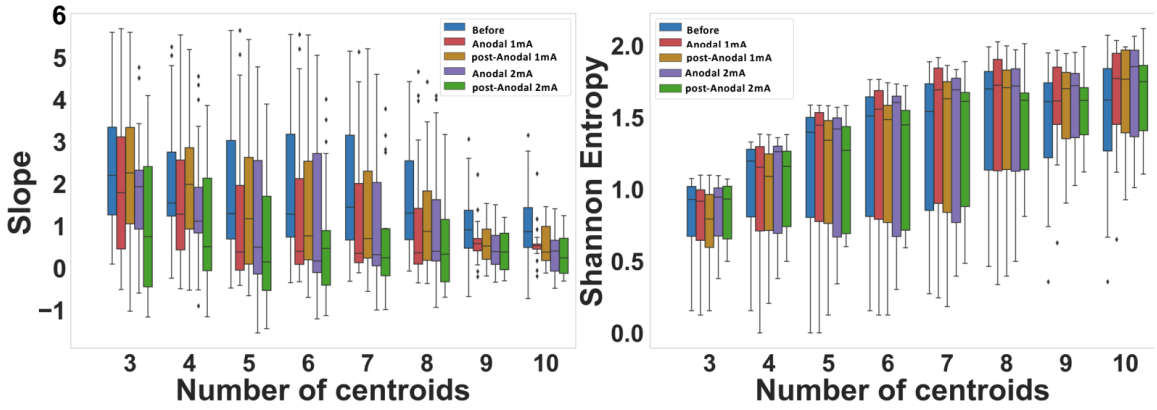

Figure 6 - figure supplement 1. Slope and Shannon Entropy in anesthesia conditions. Slopes of the linear regression (A) and Shannon Entropy (B) of the distribution of brain patterns occurrences computed for a number of clusters from 3 to 10 in the k-means algorithm. All five anesthesia conditions were included in the analyses. The same relative differences were found for all values of *k* analyzed. In the 2 mA stimulation conditions, the slopes of the linear regression are decreased compared to the pre-stimulation condition.

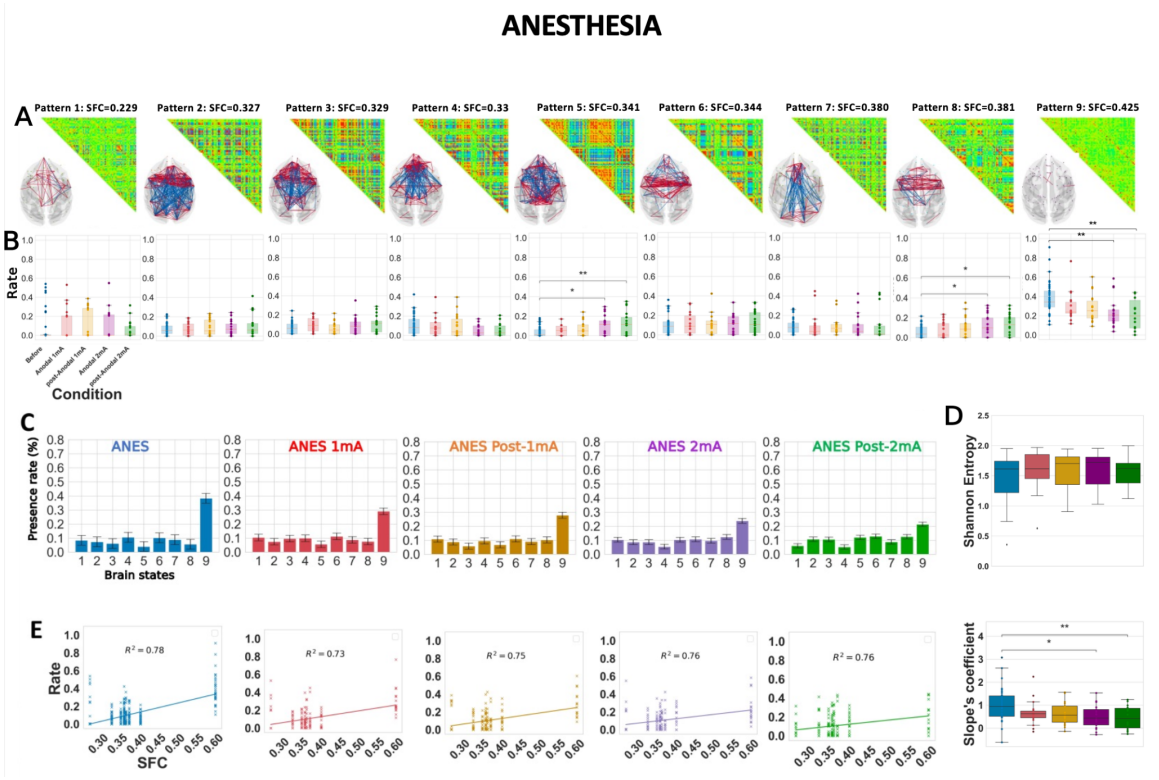

Figure 6 - figure supplement 2. Dynamical functional connectivity analysis of the anesthesia dataset with *k* = 9 numbers of clusters. Similar analysis than in Figure 7 for *k*=9 considering all the five anesthesia conditions. Before: before stimulation, under anesthesia. Anodal 1 mA, post-Anodal 1 mA: during and after anodal HD-tDCS of the PFC at 1 mA intensity. Anodal 2 mA and post-Anodal 2 mA: during and after anodal HD-tDCS of the PFC at 2 mA intensity.

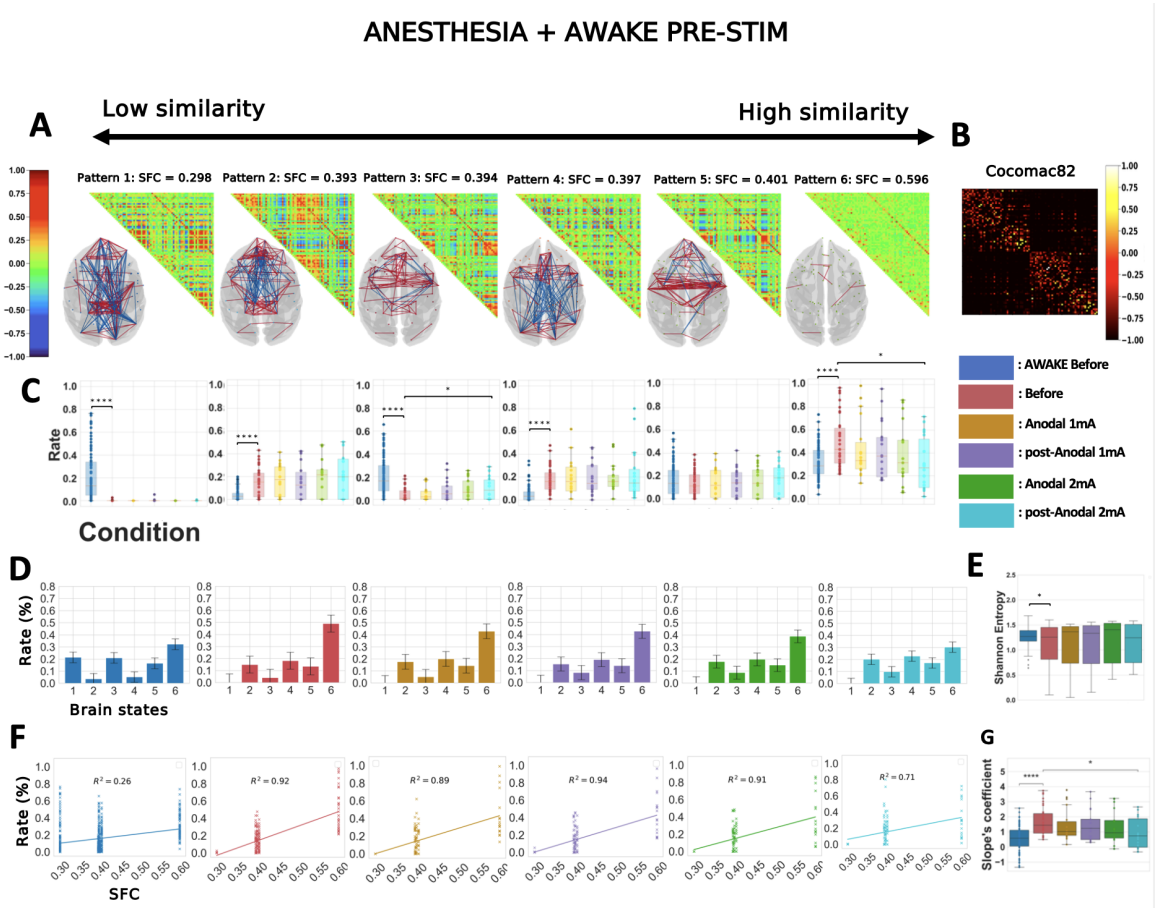

Figure 7. The effects of 2 mA anodal prefrontal HD-tDCS on anesthesia brain dynamics resist contrasting with awake dynamics. Similar analysis than in Figure 7 for *k*=6 considering all the five anesthesia conditions plus the awake pre-stimulation condition. Awake before: before stimulation in the awake state. Before: before stimulation, under anesthesia. Anodal 1 mA, Post-anodal 1 mA: during and after anodal HD-tDCS of the PFC at 1 mA intensity. Anodal 2 mA and post-Anodal 2 mA: during and after anodal HD-tDCS of the PFC at 2 mA intensity.

ANESTHESIA + AWAKE PRE-STIM

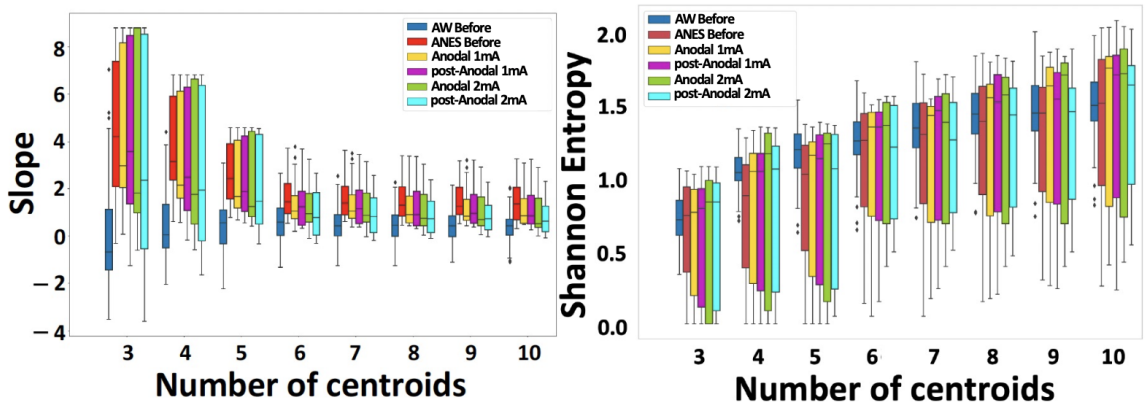

Figure 7 - figure supplement 1. Slope and Shannon Entropy in anesthesia conditions contrasted with awake pre-stimulation condition. Slopes of the linear regression (A) and Shannon Entropy (B) of the distribution of brain patterns occurrences computed for a number of clusters from 3 to 10 in the k-means algorithm. All five anesthesia conditions plus the awake pre-stimulation condition were included in the analyses. The same relative differences were found for all values of k analyzed. In the 2 mA stimulation conditions, the slopes of the linear regression are decreased and tend to approach the values of the awake pre-stimulation condition.

Tables

Table 1. Number of fMRI runs acquired in each condition for each monkey, in awake and deeply sedated states.

Awake state	**Monkey J**	**Monkey Y**
Before HD-tDCS	76	60
Anodal 2 mA HD-tDCS	32	24
Post-anodal 2 mA HD-tDCS	32	24
Cathodal 2 mA HD-tDCS	12	8
Post-cathodal 2 mA HD-tDCS	12	8

Anesthetized state	**Monkey R**	**Monkey N**
Before HD-tDCS	32	8
Anodal 1 mA HD-tDCS	16	8
Post-anodal 1 mA HD-tDCS	16	8
Anodal 2 mA HD-tDCS	16	8
Post-anodal 2 mA HD-tDCS	16	8

Table 2. Percentage of eye fixation during HD-tDCS fMRI experiments in the awake state.

Condition	Animal	Fixation (%)
Before HD-tDCS	Monkey J	99 +/- 2
	Monkey Y	98 +/- 4
Anodal 2 mA HD-tDCS	Monkey J	99 +/- 3
	Monkey Y	99 +/- 2
Post-anodal 2 mA HD-tDCS	Monkey J	98 +/- 3
	Monkey Y	98 +/- 3
Cathodal 2 mA HD-tDCS	Monkey J	99 +/- 1
	Monkey Y	100 +/- 1
Post-cathodal 2 mA HD-tDCS	Monkey J	100 +/- 1
	Monkey Y	100 +/- 1

Table 3. Physiological data during HD-tDCS fMRI experiments under deep propofol anesthesia.

Physiological parameters under deep propofol anesthesia and different HD-tDCS stimulation conditions: heart rate; oxygen saturation (SpO2); systolic blood pressure (SAP); diastolic blood pressure (DAP); respiration rate; end-tidal CO2. *: statistically significant difference compared to pre-stimulation, at $p < 0.05$ with Bonferroni correction. In brackets, the standard deviation.

Condition	Heart rate	SpO2	SAP	DAP	Respiration rate	$EtCO_2$
Before HD-tDCS	127 (10)	97 (3)	116 (11)	60 (7)	20 (2)	40 (1)
Anodal 1 mA HD-tDCS	123 (8)	98 (1)	118 (9)	60 (4)	19 (2)	40 (1)
Post-anodal 1 mA HD-tDCS	**120 (7)***	98 (1)	118 (9)	61 (4)	19 (2)	39 (1)
Anodal 2 mA HD-tDCS	**120 (7)***	98 (1)	120 (6)	63 (3)	19 (2)	39 (1)
Post-anodal 2 mA HD-tDCS	123 (4)	98 (1)	**123 (4)***	**65 (3)***	19 (2)	40 (1)

A one-way ANOVA revealed that there was a statistically significant difference in mean heart rate between at least two conditions (F(4, 111) = [3.64], p = [0.008]). The Bonferonni test for multiple comparisons found that the mean value of heart rate in the post-stimulation 1 mA and stimulation 2 mA conditions was significantly lower compared to pre-stimulation ((p = 0.024, 95% C.I. = [0.52,13.05]) and (p = 0.021, 95% C.I. = [0.62,13.15]), respectively). There was also a statistically significant difference in mean systolic and diastolic blood pressure between at least two conditions ((F(4, 131) = [2.97], p = [0.022]) and (F(4, 130) = [3.07], p = 0.018]), respectively). The Bonferonni test showed that the mean systolic and diastolic blood pressures for the 2 mA post-stimulation condition were significantly higher compared to the pre-stimulation condition ((p = 0.017, 95% C.I. = [-13.51,-0.77]) and (p = 0.033, 95% C.I. = [-8.36,-0.20]), respectively).

Table 4. Statistical analyses.

Table 4A. Awake experiments

T-test independent sample, Bonferroni correction, comparing occurrence of brain states'

Brain state #	***Compared conditions***	***Mean (SD)***	***df***	***t-value***	***Adjusted p-value***
6	Cathodal	0.50 (0.15)	95	3.0	0.013
	Before	0.37 (0.15)			
6	post-Cathodal	0.51 (0.18)	96	3.3	0.0052
	Before	0.37 (0.15)			
6	Anodal	0.33 (0.14)	51	3.7	0.002
	Cathodal	0.50 (0.15)			
6	post-Anodal	0.34 (0.18)	53	3.0	0.016
	post-Cathodal	0.51 (0.18)			
5	post-Cathodal	0.028 (0.035)	96	3.0	0.012
	Before	0.14 (0.14)			
3	Anodal	0.16 (0.12)	51	3.7	0.0022
	Cathodal	0.038 (0.046)			

Three-ways ANOVA type II

Brain state #		***Sum of Squares***	***df***	***f-value***	***p-value***
6	C(Montage)	1.8e-14	2	3.7e-13	0.99
	C(Time)	**4.2**	**2**	**84**	**<0.001**
	C(Animal)	NaN	1	NaN	NaN
	C(Montage):C(Time)	**1.1**	**4**	**11**	**<0.001**
	C(Montage):C(Animal)	6.9e-4	2	0.014	0.91
	C(Time):C(Animal)	4.6e-5	2	9.2e-4	0.97
	C(Montage):C(Time):C(Animal)	**0.99**	**4**	**9.9**	**<0.001**
	Residual	4.5	180	NaN	
5	C(Montage)	1.7e-14	2	6.5e-13	0.99
	C(Time)	0.023	2	0.87	0.35
	C(Animal)	NaN	1	NaN	NaN
	C(Montage):C(Time)	**0.17**	**4**	**3.2**	**0.04**
	C(Montage):C(Animal)	**0.24**	**2**	**9.1**	**0.0029**

	C(Time):C(Animal)	4.3e-4	2	0.016	0.89
	C(Montage):C(Time):C(Animal)	0.14	4	2.8	0.066
	Residual	2.3	180	NaN	
3	C(Montage)	2.7e-14	2	1.2e-12	0.99
	C(Time)	**0.26**	**2**	**12**	**<0.001**
	C(Animal)	NaN	1	NaN	NaN
	C(Montage):C(Time)	**0.27**	**4**	**6.1**	**0.0026**
	C(Montage):C(Animal)	0.039	2	1.8	0.18
	C(Time):C(Animal)	0.028	2	1.3	0.25
	C(Montage):C(Time):C(Animal)	0.12	4	2.6	0.07
	Residual	1.9	180	NaN	

T-test independent sample, Bonferroni correction, comparing non-normalized Shannon Entropies

Compared conditions	***Mean (SD)***	***df***	***t-value***	***Adjusted p-value***
Cathodal	1.1 (0.20)	95	2.5	0.037
Before	1.3 (0.23)			
post-Cathodal	1.1 (0.22)	96	2.5	0.04
Before	1.3 (0.23)			
Anodal	1.3 (0.23)	51	2.6	0.035
Cathodal	1.1 (0.20)			

T-test independent sample, Bonferroni correction, comparing slopes' coefficients

Compared conditions	***Mean (SD)***	***df***	***t-value***	***Adjusted p-value***
Cathodal	1.9 (0.85)	95	2.9	0.018
Before	1.0 (0.86)			
post-Cathodal	2.0 (1.0)	96	3.4	0.0043
Before	1.0 (0.86)			
Anodal	1.0 (0.80)	51	3.5	0.0038
Cathodal	1.9 (0.85)			
post-Cathodal	2.0 (1.0)	53	3.0	0.014
post-Anodal	1.0 (1.1)			

Table 4B. Markov transition

T-test independent* samples with Bonferroni correction

Transition	***Compared conditions***	***Mean (SD)***	***df***	***t-value***	***Adjusted p-value***
2 → 4	Before	0.24 (0.18)	118	2.4	0.019
	Anodal	0.16 (0.23)			
3 → 5	Before	0.056 (0.13)		3.1	0.0074
	Anodal	0.15 (0.19)			
2 → 6	Before	0.34 (0.05)		4.7	0.0018
	post-Anodal	0.47 (0.24)			
6 → 5	Before	0.24 (0.11)	95	2.7	0.043
	Cathodal	0.15 (0.16)			
5 → 2	Before	0.17 (0.11)		2.2	0.029
	Cathodal	0.10 (0.12)			
2 → 3	Before	0.19 (0.17)		2.4	0.01
	Cathodal	0.08 (0.11)			
1 → 6	Before	0.56 (0.11)		5.7	0.002
	Cathodal	0.73 (0.08)			
2 → 6	Before	0.35 (0.18)		3.6	<0.001
	Cathodal	0.66 (0.32)			
6 → 3	Before	0.15 (0.10)	96	2.3	0.024
	post-Cathodal	0.08 (0.11)			
5 → 6	Before	0.46 (0.15)		4.8	<0.001
	post-Cathodal	0.67 (0.23)			

*: Certain transitions, including transitions from brain states 4 and 5 to brain state 6, were affected both during and after cathodal stimulation. Such transitions were favored during and post-stimulation but did not pass the bootstrap and/or the ANOVA tests.

Table 4C. Awake conditions + anesthesia pre-stimulation condition

T-test independent samples with Bonferroni correction

Brain state #	***Compared conditions***	***Mean (SD)***	***df***	***t-value***	***Adjusted p-value***
4	Cathodal	0.027 (0.036)	95	2.6	0.019
	Before	0.13 (0.15)			
	post-Cathodal	0.023 (0.037)	96	2.8	0.011
	Before	0.13 (0.15)			
6	Anes Before	0.54 (0.23)	114	5.2	<0.001
	Before	0.35 (0.14)			
	Cathodal	0.47 (0.16)	95	2.9	0.021
	Before	0.35 (0.14)			
	post-Cathodal	0.48 (0.17)	96	3.1	0.0098
	Before	0.35 (0.14)			
	Cathodal	0.47 (0.16)	51	3.4	0.0049
	Anodal	0.32 (0.14)			

Two-ways* ANOVA type II

Brain state #		***Sum of Squares***	***df***	***f-value***	***p-value***
4	**C(Montage)**	**0.27**	**2**	**7.5**	**0.0065**
	C(Time)	0.094	2	2.7	0.10
	C(Montage):C(Time)	**0.37**	**4**	**5.3**	**0.0056**
	Residual	3.9	219	NaN	
6	**C(Montage)**	**4.3**	**2**	**61.0**	**<0.001**
	C(Time)	**0.63**	**2**	**8.9**	**0.0032**
	C(Montage):C(Time)	**1.1**	**4**	**7.9**	**<0.001**
	Residual	7.7	219	NaN	

*: Due to the monkeys from the anesthesia datasets being different animals than those from the awake dataset, including the animal specialness as independent variable resulted in completely NaN 3-ways ANOVA results. Hence, we removed said variable to at least verify the effect of montage type and time.

T-test independent sample, Bonferroni correction, comparing normalized Shannon Entropies

Compared conditions	***Mean (SD)***	***df***	***t-value***	***Adjusted p-value***
Before	0.73 (0.12)	95	2.3	0.049
post-Cathodal	0.65 (0.098)			
Before	0.73 (0.12)	114	7.0	<0.001
Anes Before	0.51 (0.20)			

T-test independent sample, Bonferroni correction, comparing slopes' coefficients

Compared conditions	***Mean (SD)***	***df***	***t-value***	***Adjusted p-value***
Cathodal	1.3 (0.80)	95	2.8	0.014
Before	0.69 (0.72)			
post-Cathodal	1.3 (0.85)	96	3.0	0.003
Before	0.69 (0.72)			
Cathodal	1.3 (0.80)	51	3.0	0.0072
Anodal	0.55 (0.74)			
post-Cathodal	1.3 (0.85)	53	2.6	0.023
post-Anodal	0.55 (0.74)			

Table 4D. Experiments under anesthesia

T-test independent samples with Bonferroni correction

Brain state #	***Compared conditions***	***Mean (SD)***	***df***	***t-value***	***Adjusted p-value***
2	Before	0.067 (0.070)	103	3.1	0.0035
	post-Anodal 2mA	0.17 (0.17)			
5	Before	0.084 (0.069)		2.2	0.030
	post-Anodal 2mA	0.15 (0.12)			
6	Before	0.46 (0.25)		3.1	<0.001
	post-Anodal 2mA	0.27 (0.24)			

Three-ways ANOVA type II

Brain state #		***Sum of Squares***	***df***	***f-value***	***p-value***
2	C(Montage)	-6.7e-17	2	-6.3e-15	1.0
	C(Time)	1.7e-15	2	1.7e13	1.0
	C(Animal)	**0.45**	**1**	**88**	**<0.001**
	C(Montage):C(Time)	**0.18**	**4**	**8.9**	**<0.001**
	C(Montage):C(Animal)	1.9e-17	2	1.8e-15	1.0
	C(Time):C(Animal)	-4.9e-18	2	-4.7-16	1.0
	C(Montage):C(Time):C(Animal)	**0.083**	**4**	**4.0**	**0.0047**
	Residual	0.49	95	NaN	
5	C(Montage)	-8.5e-16	2	-7.3e-14	1.0
	C(Time)	-1.1e-16	2	-9.2e-15	1.0
	C(Animal)	**0.62**	**1**	**10.6**	**<0.001**
	C(Montage):C(Time)	**0.12**	**4**	**5.3**	**<0.001**
	C(Montage):C(Animal)	1.0e-16	2	8.9e-15	1.0
	C(Time):C(Animal)	5.9-16	2	5.0e-14	1.0
	C(Montage):C(Time):C(Animal)	0.051	4	2.2	0.078
	Residual	0.56	95	NaN	
6	C(Montage)	1.9e-15	2	-4.2e-14	1.0
	C(Time)	-2.3e-16	2	-5.1e-15	1.0
	C(Animal)	**5.3**	**1**	**23.6**	**<0.001**
	C(Montage):C(Time)	**0.77**	**4**	**8.5**	**<0.001**
	C(Montage):C(Animal)	2.9e-16	2	6.4e-15	1.0
	C(Time):C(Animal)	4.9e-15	2	8.9e-14	1.0

	C(Montage):C(Time):C(Animal)	0.11	4	1.2	0.32
	Residual	2.1	95	NaN	

T-test independent sample, Bonferroni correction, comparing slope's coefficients

Compared conditions	***Mean (SD)***	***df***	***t-value***	***Adjusted p-value***
Before	1.5 (1.8)	51	2.6	0.025
post-Anodal 2 mA	0.7 (1.5)			